Published in final edited form as:
Exp Eye Res. 2013 November ; 116: . doi:10.1016/j.exer.2013.09.019.

Functional characterization of an AQP0 missense mutation, R33C, that causes dominant congenital lens cataract, reveals impaired cell-to-cell adhesion

Sindhu S. Kumari, **Jason Gandhi**, **Mohammed H. Mustehsan**, **Semih Eren**, and **Kulandaiappan Varadaraj***
Department of Physiology and Biophysics, Stony Brook University, Stony Brook, NY 11794-8661, USA

Abstract

Aquaporin 0 (AQP0) performs dual functions in the lens fiber cells, as a water pore and as a cell-to-cell adhesion molecule. Mutations in AQP0 cause severe lens cataract in both humans and mice. An arginine to cysteine missense mutation at amino acid 33 (R33C) produced congenital autosomal dominant cataract in a Chinese family for five generations. We re-created this mutation in wild type (WT-AQP0) human AQP0 cDNA by site-directed mutagenesis, and cloned and expressed the mutant AQP0 (AQP0-R33C) in heterologous expression systems. Mutant AQP0-R33C showed proper trafficking and membrane localization like WT-AQP0. Functional studies conducted in *Xenopus* oocytes showed no significant difference ($P>0.05$) in water permeability between AQP0-R33C and WT-AQP0. However, the cell-to-cell adhesion property of AQP0-R33C was significantly reduced ($P< 0.001$) compared to that of WT-AQP0, indicated by cell aggregation and cell-to-cell adhesion assays. Scrape-loading assay using Lucifer Yellow dye showed reduction in cell-to-cell adhesion affecting gap junction coupling ($P< 0.001$). The data provided suggest that this mutation might not have caused significant alterations in protein folding since there was no obstruction in protein trafficking or water permeation. Reduction in cell-to-cell adhesion and development of cataract suggest that the conserved positive charge of Extracellular Loop A may play an important role in bringing fiber cells closer. The proposed schematic models illustrate that cell-to-cell adhesion elicited by AQP0 is vital for lens transparency and homeostasis.

Keywords

AQP0; water channel; water permeability; cell-to-cell adhesion; trafficking; congenital cataract; Connexin 50

1. Introduction

Opacification of the lens or cataract accounts for about half of all cases of blindness worldwide. An estimated 20 million people suffer from bilateral cataracts; this number is

***Corresponding author**, Kulandaiappan Varadaraj, Department of Physiology and Biophysics, State University of New York at Stony Brook, BST-6, Room # 165; Stony Brook, NY 11794-8661, Phone: (631) 444-7551; Fax: (631) 444-3432, kulandaiappan.varadaraj@stonybrook.edu.

estimated to reach 32 million globally by 2020 (World Health Organization website, undated). According to the American Society of Cataract and Refractive Surgery, three million Americans undergo cataract surgery annually. Causes for cataract development include age, defects in lens proteins caused by gene mutation, diseases such as diabetes, exposure to ionizing radiation, oxidative accumulation of free radicals, or a combination of these factors.

In the adult mammalian eye, the ocular lens is a relatively transparent avascular organ that relies mainly on solute- and water channels for the distribution of nutrients and removal of metabolic waste to maintain transparency and homeostasis (Mathias et al., 1997; Robinson et al., 1983; Varadaraj et al., 1999). Aquaporins (AQPs) constitute a superfamily of small integral membrane channel proteins that allow passage of water solely, or water and certain small solutes across the plasma membranes, depending on the osmotic gradient. In mammals, the superfamily comprises 13 isoforms (AQP0-12). Among them, three aquaporin water channels are expressed in the lens, namely AQP0, AQP1 and AQP5. AQP0 is expressed abundantly in the fiber cell membrane (Bassnett et al., 2009; Broekhuyse et al., 1976; Chepelinsky, 2009; Shiels et al., 2001; Varadaraj et al., 2007). AQP1 is expressed in the monolayer of epithelial cells (Hamann et al., 1998; Varadaraj et al., 2005, 2007) and AQP5 is expressed in both epithelial and fiber cells (Bassnett et al., 2009; Grey et al., 2013; Kumari et al., 2012).

In the lens, AQP0 facilitates water permeation (Shiels, 2012; Shiels et al., 2001; Tong et al., 2013; Varadaraj et al., 1999, 2005, 2010;) and cell-to-cell adhesion (Kumari and Varadaraj, 2009; Buzhynskyy et al., 2007; Costello et al., 1985; Kumari et al., 2011; Liu et al., 2011; Michea et al., 1994,1995; Scheuring et al., 2007; Varadaraj et al., 2010). AQP0 has a molecular mass of ~28 kDa, six putative transmembrane domains, and two half-membrane-spanning domains (Fig. 1A). Three extracellular (A, C, and E) and two intracellular loops (B and D) serve as connectors of transmembrane domains. Highly conserved NPA motifs that line the water pore of aquaporin are located in loops B and E. The amino and carboxyl termini are intracellular with respect to the plasma membrane (Gonen et al., 2004, 2005; Harries et al., 2004). Molecular and structural studies confirmed that aquaporins are functional only in the tetrameric form in the membrane (Cheng et al., 1997; Murata et al., 2000; Ren et al., 2000; Walz et al., 1997). However, each subunit functions as a water channel.

AQP0 mutations identified thus far invariably resulted in autosomal dominant lens cataracts, underlining the importance of this protein for lens transparency. To date, eleven such mutations in human (Table 1a; Fig. 1B) and four in mice have been reported (Table 1b; Fig. 1B). Gu et al. (2007) identified a mutation in a five-generation Chinese family with autosomal dominant congenital lens cataract. Sequencing of the coding regions of AQP0 revealed a point mutation at codon 33 resulting in substitution of a cysteine (C) for arginine (R). This is the first point mutation identified in the putative Extracellular Loop A of AQP0 that caused total lens cataract (Fig. 1B). The Extracellular Loop A has been speculated to play a role in cell-to-cell adhesion (Michea et al., 1994, 1995; Gonen et al., 2004; Harries et al., 2004).

The present study was undertaken to find out whether the substitution of positively charged amino acid arginine (R33) in the Extracellular Loop A of AQP0 with a neutral cysteine (C) altered water permeation and/or cell-to-cell adhesion causing lens cataract. We performed heterologous expression of the human wild type (WT-AQP0) and mutant AQP0 (AQP0-R33C) in *Xenopus* oocytes as well as in Madin–Darby Canine Kidney (MDCK) cells and adhesion-deficient L-cells.

Results show that loss of arginine at position 33 to cysteine did not influence protein trafficking and water channel function. However, it caused a significant reduction in cell-to-cell adhesion. As a secondary effect, reduction in cell-to-cell adhesion of fiber cells affected gap junction coupling and intercellular communication. Our data pointing out the contribution of the conserved positive charge for establishing firm adherence of fiber cells suggest that cell-to-cell adhesion exerted by AQP0 is critical for lens transparency and homeostasis.

2. Materials and methods

2.1. Construction of plasmids that encode E-Cadherin, WT-AQP1, WT-AQP0 or AQP0-R33C

Expression constructs were generated with or without a fluorescent tag (mCherry, a gift from Dr. Roger Y. Tsien, University of California, San Diego; EGFP, Clontech, Mountain View, CA) at the C-terminal end of AQP0 and cloned into pcDNA 3.1 myc-His vector (Invitrogen, CA) carrying CMV and T7 promoters for *Xenopus* oocyte and mammalian cell expressions, as described previously (Varadaraj et al., 2008). In short, the coding sequence of wild type human AQP0 with or without a C-terminal tag was amplified by PCR, gel purified and cloned in the aforementioned vector and used for creating the point mutation at amino acid 33 (R33C; Gu et al., 2007). Using QuickChange site-directed mutagenesis kit (Stratagene, La Jolla, CA) and specific oligonucleotides, the mutation of arginine at position 33 to cysteine (R33C) was incorporated in the wild type constructs (Varadaraj et al., 2008). The following sense and antisense primers were used: 5′- GTC CTC ACT GTG CTG GGC TCC-3′ (sense) and 5′- GGA GCC CAG CAC AGT GAG GAC −3′ (antisense). The introduced mutation as well as the entire insert sequence was confirmed by bidirectional automated sequencing at our University sequencing facility. WT-AQP1 and E-Cadherin expression constructs previously used (Kumari and Varadaraj, 2009) were included in experiments as necessary.

2.2. cRNA expression in *Xenopus* oocytes

Capped complementary RNAs (cRNAs) were synthesized *in vitro* using T7 RNA polymerase (mMESSAGE mMACHINE T7 Ultra Kit, Ambion, USA). The cRNAs were quantified using a NanoDrop spectrophotometer (ND-2000c, ThermoFisher, MA) and aliquots were stored at −80°C. Ovarian lobes contai ning stage V and VI oocytes were surgically removed from *Xenopus laevis* frog and defolliculated using Collagenase Type II (Sigma). The oocytes were maintained at 18°C, an d 5 or 25 ng cRNA of the respective expression construct was injected in a volume of 25 nl/oocyte (Varadaraj et al., 2008). An equal volume of distilled water was injected for control oocytes.

2.3. Immunostaining and western blotting of AQP0 proteins expressed in oocytes

Cryosections (thickness:12–18μm) were made of *Xenopus laevis* oocytes injected with distilled water (control) or expressing WT-AQP0 or AQP0-R33C protein, and immunostained with polyclonal rabbit antibody raised against human AQP0 (Santa Cruz Biotechnology, Inc., Dallas, TX). The processed sections were mounted in anti-fade Vectamount (Vector Laboratories, Inc., Burlingame, CA). Optimized Z-sectional digital images were acquired using Zeiss Axiovert 200M motorized inverted fluorescence microscope (Varadaraj et al., 2008).

Oocytes were tested to verify translation of injected human WT-AQP0 and mutant AQP0-R33C cRNA by western blot analysis. For sample preparation, WT-AQP0 or AQP0-R33C cRNA injected oocytes were suspended in 500 μl of lysis buffer containing 5 mM Tris (pH 8.0), 5 mM EDTA and protease inhibitors (Sigma Chemicals, St. Louis. MO). The oocytes were lysed using a sequence of mechanical passages through 20, 22, 24 and 26 Gauge

hypodermic needles. The lysates were centrifuged at 800 X g at 4 °C for 5 minutes. The supernatant was c entrifuged at 100,000 X g at 4 °C for 45 min. Membrane pellets were treated with 2X SDS-PAGE loading buffer and sonicated on ice. The samples were heated to 55−60°C for 10 min. to facilitate complete dissolution of membrane pellets, and resolved on a 4−12% SDS-polyacrylamide gradient gel. Western blotting was performed using a C-terminal- specific anti-AQP0 antibody (Varadaraj et al., 2007, 2008).

2.4. Expression and localization of WT-AQP0 and AQP0-R33C proteins in cultured cells

MDCK and mouse fibroblast L-cells (CCL-1.3) from ATCC (Manassas, VA) were cultured in a 37°C incubator set with 5% CO_2. WT-AQP0-mCherry and AQP0-R33C-EGFP expression constructs were transfected separately using Effectene reagent (Qiagen, USA) or X-tremeGENE HP DNA transfection reagent (Roche Diagnostics, Indianapolis, IN) according to the company protocols. Fluorescent signals were captured using a Zeiss epifluorescent microscope equipped with mCherry and EGFP fluorescent filters.

Colocalization studies were performed as described by Varadaraj et al. (2008) to find out whether WT-AQP0-mCherry and AQP0-R33C-EGFP could colocalize at the membrane. Briefly, MDCK cells were cotransfected with WT-AQP0-mCherry and mutant AQP0-R33C-EGFP expression plasmid constructs, and grown on sterile coverslips. After fixing in 4% paraformaldehyde, coverslips were washed with PBS and mounted on slides using anti-fade Vectamount with DAPI nuclear stain. Fluorescent signals from cotransfected WT-AQP0-mCherry and mutant AQP0-R33C-EGFP were captured separately using a Zeiss epifluorescent microscope with mCherry and EGFP fluorescent filters. Images of the fluorescent signals were superimposed (Varadaraj et al., 2008).

Forster Resonance Energy Transfer (FRET) technique was employed for tracing colocalization. We used AQP0-R33C-EGFP as the donor (Ex 488 and Em 507) and WT-AQP0-mCherry as the acceptor (Ex 587 Em 610). Images were acquired using a Zeiss microscope fitted with a 63x oil immersion lens, and equipped with the following filters/ dichroic sets (nm): (1) Texas Red cube, excitation (EX) 545/30, emission (EM) 620/60, beamsplitter 570 (longpass); (2) EGFP cube, excitation (EX) 470/40, emission (EM) 525/50, beamsplitter 495 (longpass); (3) FRET cube, EX 470/40, EM 640/50, beamsplitter 495 (longpass) (Chroma Technology Corp, USA). As a control, WT-AQP0-mCherry and WT-AQP0-EGFP were co-transfected and subjected to FRET analysis.

To test endoplasmic reticulum (ER)-specific and membrane-specific localization, MDCK cells expressing WT-AQP0-EGFP and mutant AQP0-R33C-EGFP were seeded onto a 35 mm culture dish with square coverslips and grown to 100% confluence. To highlight the ER, cells were transduced with Organelle Light Intracellular Targeted Fluorescent Protein, ER-Red Fluorescent Protein (ER-RFP, BacMam 1.0), as described by the manufacturer (Invitrogen). The cells were gently washed twice with pre-warmed normal growth medium, replaced with fresh medium and imaged 36h post-transfection. Washing of the cells was done in warm 1X PBS. The cells were fixed in 4% paraformaldehyde and washed again. The glass coverslips with cells were mounted in anti-fade Vectamount containing DAPI nuclear stain. Cells were imaged using Caral Zeiss AxioVision Confocal microscope. Optimized Z-sectional digital images were acquired as described above.

Western blotting of cells expressing WT-AQP0-mCherry and AQP0-R33C-EGFP was carried out as described (Varadaraj et al., 2008).

2.5. Oocyte membrane water permeability measurement

Oocyte membrane water permeability (Pw, μm/s) was calculated from rate of swelling of the control (distilled water-injected) and cRNA of WT-AQP0- and/or mutant AQP0-R33C-

injected oocytes in response to hypo-osmotic shock, as described previously (Varadaraj et al., 1999, 2005, 2008). Two days after the injections, membrane permeability assay was performed and Pw was quantified from the initial slope of the volume change when oocytes were subjected to an osmotic gradient from 180 to 60 mOsm at 20°C. Pw was calculated using the formula, $Pw = (dV/dt)/(S_m V_w \Delta c)$, where V ($cm^3$) is the oocyte volume calculated from the cross-sectional area, S_m (cm^2) is the oocyte surface area calculated from the cross-sectional area, V_w is the molar volume of water (18 cm^3/mol) and Δc is the change in bath osmolarity (0.12×10^{-3} mol/cm^3).

2.6. Cell-to-cell adhesion studies

2.6.1. Cell aggregation assay using a rotary gyratory shaker—Cell aggregation assay was performed as described previously (Vicker and Edwards, 1972; Takeichi, 1977; Takahashi, et al., 1999; Andl et al., 2003; Hiroaki et al., 2006; Kumari and Varadaraj, 2009). This assay is a semi-quantitative measurement of proteins that promote cell-to-cell adhesion; it does not measure the amount of adhesive force involved. However, a protein that promotes strong adhesion would show more cell clustering and firm adhesion at a given time and *vice versa*. Clones of L-cells stably expressing empty vector, AQP1, (negative controls), E-cadherin (positive control), WT-AQP0, AQP0-R33C and WT-AQP0 + AQP0-R33C were grown to 75–85% confluence. After gentle washing with 1X PBS without Ca^{2+}, single cell preparations were made by trypsinization and dispersion by gentle pipetting. Additional washing of the cells two times with 1X PBS without Ca^{2+} was followed by a final wash using serum-free Opti-MEM I and the cells in each group were suspended in serum-free Opti-MEM I.

Before beginning the cell aggregation assay, initial cell numbers were counted using a hemocytometer. First, the hemocytometer was pre-coated with 2% bovine serum albumin (BSA) to prevent attachment of cells to the glass. After gentle mixing, an aliquot of cells from a group was added to the hemocytometer using a nonstick pipette. Cells were counted under an Olympus light microscope set to use a phase contrast objective. Cell counting was performed for each sample. Samples were diluted to 1×10^5 cells per ml and 2.5 ml of each cell suspension was plated separately in 6-well plates, pre-coated with 2% agarose (Sigma) or 2% BSA (Sigma-Aldrich, St. Louis, MO) to prevent attachment of cells to the plastic, and rotated on a rotary gyratory shaker (80 rpm) for 30, 60 and 90 min, at 37°C. At the end of each time period, an equal volume of 2% glutaraldehyde was added to stop further cell-to-cell aggregation, or dissociation of aggregates. Particle number was determined using a hemocytometer. A particle by definition is a single cell or one cell-aggregate (two or more cells sticking together). A minimum of five aliquots were counted for each sample and time point, and resulting values were averaged. At the end of a given time depending on the tendency to aggregate, the samples would show less number of particles as a result of cell aggregation compared to the number of particles at the beginning of the experiment. The extent of aggregation (EA) at various intervals was calculated from the ratio of total number of particles at time 't' of incubation (N_t) to the initial number of particles at the start of the assay (N_0), and expressed as percentage ($EA\ (\%) = (N_t/N_0)\times100$). EA would be inversely proportional to the number of particles. The aggregation assay was repeated six times and the mean and standard deviations calculated were plotted as a graph.

2.6.2. Cell-to-cell adhesion assay using a microplate reader—The adhesion assay was based on the novel procedure using a microplate reader reported previously from our laboratory (Kumari and Varadaraj, 2009). This assay measures semi-quantitatively the adhesion efficiency of a protein that promotes cell-to-cell adhesion. This method does not directly measure the amount of adhesive force involved.

Adhesion-deficient mouse L-cells expressing empty vector, AQP1, E-cadherin, WT-AQP0, mutant AQP0-R33C or WT-AQP0 + mutant AQP0-R33C at 75–85 % confluence were incubated with 5 μM/ml CellTracker™ Red CMPTX dye (Invitrogen, CA) in serum-free Opti-MEM I with 1% BSA for 1 h. After washing with 1X PBS, the dye-loaded cells were incubated for 30–45 min in MEM containing 10% FBS, collected by trypsinization at 21°C for 3 min, neutralized wi th MEM containing 5% FBS, washed three times with 1X PBS containing 1% BSA, and suspended in serum-free Opti-MEM I containing 1% BSA. In 24-well microplates, a monolayer of confluent L-cells stably expressing vector, AQP1, E-cadherin, WT-AQP0, AQP0-R33C or WT-AQP0+mutant AQP0-R33C was maintained separately. Cells were prepared as given in section 2.6.1, counted and diluted to 1×10^5 per ml. A 250 μl aliquot of the respective CellTracker-Red-loaded L-cell suspension was smoothly added to each matching group and gently agitated for uniform distribution over the attached cell lawn. Cells were incubated for 1h at 37°C and fluorescence was measured at excitation /emission wavelengths of 584/612 nm. Cells were gently washed three times with serum-free MEM culture medium containing 1% BSA for 5 min each and one time with 1XPBS on a rotary shaker at 40 rpm, at room temperature, to remove non-adhered and weakly adhered cells. More cells would remain attached to the lawn of cells if the expressed protein had strong adhesive property and *vice versa*. Non-adherent cells were removed and fluorescence was read again as described above. The ratio between fluorescence intensity (FI) of CellTracker-Red loaded cells that remained adhered after washing (FIAW) and that of CellTracker-Red loaded cells post-incubation before washing (FIBW) expressed as percentage of fluorescence intensity (**PFI** (%) = [(FIAW/FIBW)×100]), was considered as the measure of the cell-to-cell adhesion elicited by each sample. For different stages of the experiment, such as reading initial fluorescence of total cells loaded and fluorescence due to adhered cells, a minimum of 10 wells were used and values were averaged. Relative adhesion (**RA)** of the protein of interest normalized to E-Cadherin positive control was calculated as the ratio between the PFI of cells expressing the protein of interest (PFI of protein of interest) and the PFI of cells expressing E-cadherin positive control (PFI of E-cadherin) and expressed as percentage (RA (%) = (PFI of Protein of interest) / (PFI of E-cadherin) x 100). The assay was repeated four times, mean and standard deviations were calculated, and represented as a bar graph. The statistical significance of the difference between two samples (e.g. WT-AQP0 vs mutant R33C) was determined by the paired *t*-test using data obtained from four experimental replications. $P < 0.05$ was considered significant.

2.6.3. Cell-to-cell adhesion assay using an epifluorescent microscope—In this assay, all the steps followed were the same as in section 2.6.2., except a fluorescent imaging technique using a Zeiss epifluorescent microscope was used instead of a microplate fluorescence intensity reader. The attached cells were counted and the relative cell-to-cell adhesion efficiency was calculated with reference to the positive control E-cadherin and expressed as percentage.

In brief, adhesion-deficient L-cells stably expressing empty vector, AQP1, E-cadherin, WT-AQP0 or mutant AQP0-R33C grown to 80% confluence were loaded with membrane permeable CellTracker™ Red CMPTX dye as described above in section 2.6.2 dissociated by trypsinization at 21°C for 3 m in, neutralized, washed, counted using a hemocytometer pre-coated with 2% BSA, and suspended in serum-free MEM culture medium containing 1% BSA. Equal numbers of the dye-loaded cells were added to a monolayer of L-cells cultured in 24-well microplates, and stably expressed the respective protein but were not dye-loaded. After 45 min of incubation at 37°C, cells were gently washed three times with serum-free MEM culture medium containing 1% BSA for 5 min each on a rotary shaker at 40 rpm at room temperature to remove loose and weakly adhered cells. More cells would attach to the lawn of cells if the expressed protein had strong adhesion property; less number

or no cells would attach to the lawn of cells if the expressed protein had weak or no adhesive property. The cells were fixed in 2% glutaraldehyde to stop further cell adhesion or dissociation. Cells were imaged under a Zeiss epifluorescent microscope and the number of fluorescent cells adhered to the cell lawn was counted for each group. The assay was repeated five times. Relative adhesion (RA) normalized to positive control E-cadherin was calculated as the ratio between the number of fluorescent cells (NFC) expressing the protein of interest that adhered to the cell lawn after washing (NFC of Protein of interest) and number of fluorescent cells expressing E-cadherin positive control at adhered to the cell lawn after washing (NFC of E-cadherin) and expressed as percentage (RA (%) = (NFC of Protein of interest) / (NFC of E-cadherin) × 100). RA values of five repeats were used to calculate the mean and standard deviations and were represented as a bar graph. The statistical significance of difference between two samples was determined by the paired *t*-test using data from the five experimental repeats. $P < 0.05$ was considered significant.

2.7. Gap junction coupling functional assay using scrape-loading dye transfer

Expression construct for rat Cx50 was generated without a fluorescent tag in pcDNA 3.1 myc-His vector (Invitrogen, CA) carrying CMV and T7 promoters as described previously (Varadaraj et al., 2008). The coding sequence of wild type rat Cx50 was amplified by PCR, gel purified and cloned into the vector. The insert sequence was confirmed by automated sequencing at our University Sequencing Facility. Expression construct was transfected in adhesion deficient L-cells and expression clones were selected using G418 and expression was confirmed by western blotting using Cx50 specific antibody (K-20; Santa Cruz Biotechnology, Inc., TX). Cells propagated from a single clone expressing Cx50 were used to transfect WT-AQP0 and AQP0-R33C expression constructs described in section 2.4. and expression clones were selected using G418 and confirmed by western blotting using AQP0 specific antibody as in section 2.3. Equal amount of WT-AQP0 and AQP0-R33C protein expressing clone for each was selected for scrape-loading dye transfer assay. Scrape loading dye transfer assay was used to simultaneously test dye coupling in a large population of cells. Briefly, stable cell lines expressing empty vector, WT-AQP0, AQP0-R33C, lens connexin 50 (Cx50), or Cx50 + WT-AQP0 or Cx50 + AQP0-R33C were plated on 24-well culture plates 24h prior to scrape-loading. After rinsing with Hank's balanced salt (HBS) solution, 0.5 ml of PBS solution containing 5 mg/ml of Lucifer Yellow CH (LY, MW 457.25; Sigma–Aldrich, St. Louis, MO) was added to the cells. Two longitudinal scratches were made through the cell monolayer using a 27-gauge needle. After 5 min, the cultures were rinsed with HBS and incubated for 30 min., to allow dye transfer to adjoining cells via gap junction channels. The cells were rinsed with 1XPBS, fixed with 4% paraformaldehyde, and viewed using Zeiss Axiovert 200M inverted epifluorescence microscope using FITC filter. Images were captured and digitized. The degree of LY dye transfer was quantified by measuring the distance from the scrape lines to the travel front of LY. At least five images for each scrape wound per well, and six wells per sample, were used to assess the level of dye transfer. Distance covered by intercellular LY transfer would be directly proportional to the number of coupled cells.

2.8. Statistics

Student's paired t-test was performed using Sigma Plot 2000 software, Version 6.10. A value of $P \leq 0.05$ was considered significant.

3. Results

Using heterologous expression systems, we sought to characterize the impact of AQP0-R33C mutation in membrane trafficking and functional expression. We used two such

expression systems, namely *Xenopus laevis* oocytes and mammalian cells to conduct experiments.

3.1. Expression and localization of WT-AQP0 and mutant AQP0-R33C

The first question put forth was whether mutant AQP0-R33C can traffic to the membrane. To find out, experiments were designed to study protein expression and localization. We synthesized cRNAs of WT-AQP0 and AQP0-R33C *in vitro*. *Xenopus* oocytes were injected with 25 ng cRNA of WT-AQP0 or AQP0-R33C; distilled water injected oocytes served as control. After allowing enough time for protein expression, oocytes were cryosectioned and immunostained with anti-AQP0 antibody. Expression and localization of WT-AQP0 and AQP0-R33C were studied using confocal microscopy. As anticipated, there was no specific immunostaining in water-injected oocytes (Fig. 2a). It is interesting to note that both WT-AQP0 (Fig. 2b) and AQP0-R33C (Fig. 2c) proteins localized at the oocyte plasma membrane. Patterns of expression and localization of AQP0-R33C were not significantly different from those of WT-AQP0, indicating that the mutation did not impair membrane trafficking.

To further confirm expression of the respective proteins in the oocyte plasma membrane, immunoblot analysis of total membrane proteins extracted from oocytes injected with WT-AQP0 or AQP0-R33C cRNA was performed. Both samples verified expression of corresponding proteins by immunoreactivity to an expected peptide band size of ~28 kDa (Fig. 2d).

Expression and localization were also tested in culture cells. WT-AQP0-mCherry and mutant AQP0-R33C-EGFP were transfected separately or together into MDCK cells. WT-AQP0-mCherry (Fig. 3a) and mutant AQP0-R33C-EGFP (Fig. 3b) chimeric proteins localized abundantly at the plasma membrane, as seen at the oocyte plasma membrane (Fig. 2b, c). Immunoblotting of proteins extracted from cells transfected with respective expression constructs showed anti-AQP0 antibody binding to a ~58 kDa band for WT-AQP0-mCherry and mutant AQP0-R33C-EGFP (Fig. 3c). When WT-AQP0-mCherry and mutant AQP0-R33C-EGFP were cotransfected, both chimeric proteins coexpressed profusely at the plasma membrane (Fig. 3d, e). Images of WT-AQP0-mCherry and AQP0-R33C-EGFP, taken from the same cell were superimposed to verify colocalization of wild type and mutant proteins. The yellow signal that emerged when the images were merged reinforced their colocalization (Fig. 3f).

Aquaporin proteins are synthesized and assembled as tetramers in the ER (Aerts et al., 1990; Buck et al., 2007; Konig et al., 1997; Smith and Agre, 1991; Zampighi et al., 1989). To determine whether WT-AQP0-mCherry and AQP0-R33C-EGFP proteins could assemble as tetramers and colocalize in the ER, both expression constructs were cotransfected into MDCK cells and subjected to FRET analysis with EGFP serving as the donor fluorophore and mCherry as the acceptor (Fig 4a–c). As a control, we cotransfected WT-AQP0-mCherry and WT-AQP0-EGFP and performed FRET analysis (Fig. 4d–f). Figure 4c shows the emerged FRET signal, suggesting colocalization of wild type and mutant proteins in the same oligomer as heterotetramers or within 100Å; Figure 4f supports the soundness of the technique by providing FRET signal for the wild type cloned and expressed separately with two different fluorophores (Fig. 4 d, e).

To confirm that WT-AQP0 and AQP0-R33C localize at the ER and plasma membrane, an ER organelle-specific test was conducted. Confluent MDCK cells grown on coverslips were coexpressed with Organelle Light ER-RFP + WT-AQP0-EGFP or ER-RFP + AQP0-R33C-EGFP (Fig. 4g – l). Cells were viewed under the EGFP filter to show membrane localization (Fig 4 g, j). The cells were viewed under Texas Red filter to highlight ER-specific

localization (Fig.4 h, k). The respective images for wild type (g, h) and mutant (j, k) were merged. The red and green merged-image turned yellow, indicating localization of proteins in the ER (Fig. 4 i, l). The green signal, visible mostly at the periphery, highlights expression of the respective protein along with the attached EGFP at the plasma membranes (Fig. 4 i, l). This experiment showed that the mutant AQP0-R33C can traffic via ER and localize at the plasma membrane like the WT-AQP0.

3.2. Functional expression of WT-AQP0 and AQP0-R33C proteins

We studied water permeability (Pw) of *Xenopus* oocytes injected with distilled water, or 25 ng cRNA of WT-AQP0 or AQP0-R33C as given in the 'Materials and Methods' section. WT-AQP0 and AQP0-R33C were tested with and without a C-terminal fluorescent tag. Distilled water injected oocytes were treated as a control. AQP1-injected oocytes (5 ng) served as a positive control. There was no functional abnormality due to the attachment of a C-terminal tag as was evident from comparable values of water permeability obtained for AQP0 proteins expressed with and without a tag for the wild type and the mutant (Fig. 5 B). Similar results had been observed and reported previously (Varadaraj et al., 2008; Yang and Verkman, 1997). Both the WT-AQP0 and AQP0-R33C injected oocytes provided overlapping values for the relative volume increase (Fig. 5A, B) indicating the mutation did not compromise the water channel function of AQP0. As expected, the relative volume (Fig. 5A) of AQP1-injected oocytes was highest, reflecting the water channel's much higher efficiency. Pw of oocytes injected with distilled water was 11.8 ± 3.5 μm/s while that of WT-AQP0 was 27.3 ± 5.4 μm/s, and of AQP0-R33C, 26.7± 4.8 μm/s. The Pw of the mutant AQP0-R33C was not significantly different from that of WT-AQP0 (Fig. 5B), indicating that the mutation did not affect water channel function. Also, when the WT-AQP0 and AQP0-R33C were co-expressed, the oocyte plasma membrane Pw was not altered significantly compared to that of WT-AQP0 ($P > 0.05$; also, Fig. 5B).

3.3. Cell-to-cell adhesion property of WT-AQP0 and AQP0-R33C

AQP0-R33C showed proper trafficking and membrane localization as the WT-AQP0 (Figs. 3, 4). It also retained normal water channel function. These two observations and the positioning of this cataract-causing mutation at a putative extracellular loop prompted us to test the cell-to-cell adhesion efficiency of AQP0-R33C. Mouse L-fibroblast cells lacking endogenous cell adhesion molecules were stably transfected with vector (negative control), AQP1 (negative control), E-cadherin (positive control), WT-AQP0, mutant AQP0-R33C or WT-AQP0 + AQP0-R33C and individual clones were selected using G418. Clones that showed very high levels of expression were selected for further studies.

Cell-to-cell adhesive property was tested using cell aggregation assay in a rotary gyratory shaker. Cells expressing E-cadherin, WT-AQP0 or mutant AQP0-R33C displayed considerable cell aggregation as a function of time (Fig. 6A). As time progressed, more and more E-cadherin, WT-AQP0 and mutant AQP0-R33C transfected cells formed cell clusters, consequently reducing the number of non-aggregating individual L-cells. E-cadherin served as a positive control (Kumari and Varadaraj, 2009; Yap et al., 1997) which was used as a standard to calculate relative aggregation by other proteins. The extent of aggregation exhibited by WT-AQP0 was 18% more than that of mutant AQP0-R33C (Fig. 6A). Cells transfected with empty vector or AQP1 did not show considerable aggregation with passage of time. Lack of cell cluster formation by AQP1 indicated absence of cell-to-cell adhesion capability which had also been reported by Hiroaki et al. (2006). Cells cotransfected with WT-AQP0 and AQP0-R33C showed more aggregation (Fig. 6A) compared to those transfected with only AQP0-R33C, and less aggregation compared to cells transfected with WT-AQP0, suggesting mutation-induced reduction in the cell aggregation capability (Fig. 6A).

To mimic and estimate lens fiber cell-to-cell adhesion promoted by WT-AQP0 and mutant AQP0-R33C, a novel method developed previously by our laboratory (Kumari and Varadaraj, 2009) was used. Mouse fibroblast L-cells stably expressing empty vector, negative control AQP1, positive control E-Cadherin, WT-AQP0, AQP0-R33C or WT-AQP0 + AQP0-R33C grown to 75–85% confluence were subjected to the assay. Relative adhesion induced by each protein was estimated using E-Cadherin as a positive control. Cell-to-cell adhesion induced by WT-AQP0, AQP0-R33C or WT-AQP0 + AQP0-R33C expressing cells was statistically significant ($P < 0.001$; Fig. 6B) compared to negative controls, L-cells expressing empty vector or AQP1. WT-AQP0, AQP0-R33C or WT-AQP0 + AQP0-R33C showed significantly less cell-to-cell adhesion ($P < 0.001$) compared to L-cells expressing the positive control E-Cadherin (Fig. 6B). The important finding of this study is the reduction in cell-to-cell adhesion observed for mutant R33C–AQP0 (~27%) compared to the WT-AQP0. There was statistically significant reduction in cell-to-cell adhesion for mutant AQP0-R33C (**$P < 0.001$) and WT-AQP0 + AQP0-R33C (***$P < 0.05$) expressing cells compared to the WT-AQP0 expressing cells.

To further investigate cell-to-cell adhesion, a fluorescence imaging assay developed in our laboratory (Kumari and Varadaraj, 2009) was used (Fig. 6C). CellTracker™ Red CMPTX dye-loaded cells of empty vector, AQP1, E-Cadherin, WT-AQP0 and AQP0-R33C were added to corresponding unloaded cells and cells that remained attached after washing were imaged using an epifluorescent microscope (Fig. 6C). The dye-loaded cells in the images were counted as described in the ‘Materials and Methods’ section, and plotted (Fig. 6D). Cell-to-cell adhesion induced by WT-AQP0 or mutant AQP0-R33C expressing cells was statistically significant ($P < 0.001$; Fig. 6D) compared to L-cells expressing empty vector or AQP1. Adhesion efficiency of cells expressing WT-AQP0 was significantly less (*$P < 0.001$) compared to the positive control cells expressing E-Cadherin (Fig. 6D). The cell-to-cell adhesion exerted by the mutant AQP0-R33C was significantly lower (34%) than that of the WT-AQP0 (** $P < 0.0001$; Fig. 6D). Results of this cell-to-cell adhesion study using the fluorescence imaging technique (Fig. 6D) followed a similar pattern to that obtained in the cell-to-cell adhesion assay using a microplate reader (Fig. 6B).

3.4. Effect of AQP0-R33C mutation on Cx50 gap junction coupling

AQP0 forms thin junctions due to its cell-to-cell adhesion property. Electron microscopic studies revealed presence of connexin clusters near AQP0 square arrays (Buzhynskyy et al., 2007). Using chicken embryonic fibroblast cells, Liu et al. (2011) demonstrated that cell-to-cell adhesion facilitated by AQP0 enhanced the Cx50-mediated gap junction coupling for intercellular communication. In order to find out whether the reduction in cell-to-cell adhesion in the human mutant AQP0-R33C could affect intercellular communication, we tested Cx50-mediated cell-to-cell dye coupling. For this experiment, Cx50 construct was transfected into L-cells and clone selection was performed under G418 to ensure stable expression. A clone that expressed considerable level of Cx50 was selected after performing western blotting (Fig. 7Aa). Cells propagated from this clone were used to transfect WT-AQP0 and AQP0-R33C constructs. Comparable amount of WT-AQP0 or AQP0-R33C expression in Cx50 expressing L-cells was verified by Western blotting (Fig. 7Ab).

L-cells stably expressing vector (negative control), WT-AQP0, AQP0-R33C, rat Cx50, WT-AQP0 + Cx50, or AQP0-R33C + Cx50 were tested using Scrape-loading Lucifer Yellow (LY) dye transfer technique, which permits real-time observation of cell-to-cell dye coupling due to functional gap junction channel formation (El-Fouly et al., 1987; Liu et al., 2011; Opsahl and Rivedal, 2000; Venance et al., 1995). Cell-to-cell-mediated dye coupling levels were evaluated from the distance of LY dye migration (Fig. 7A). LY spread in the monolayer of cells would be directly proportional to the number of coupled cells. Dye

transfer in the cells transfected with WT-AQP0 or AQP0-R33C was not significantly different from vector-transfected cells (Fig. 7A). The dye transfer in the cells transfected with Cx50 alone was less than that of the cells expressing Cx50 + WT-AQP0 or Cx50 + AQP0-R33C. However, the distance of dye migration was less in cells expressing AQP0-R33C + Cx50 compared to cells expressing WT-AQP0 + Cx50, indicating that the mutation weakened cell-to-cell adhesion capability of AQP0 and compromised gap junction coupling. The level of dye-coupling was semi-quantified by measuring the distance of LY-dye migration from the scrape line to the dye front, and plotted as a graph (Fig. 7B). Cells coexpressing rat Cx50 and WT-AQP0 showed an increase (40%) in LY-dye transfer over those expressing only Cx50 (*$P < 0.001$), implying facilitation of gap junction coupling by AQP0. However, the level of dye-coupling in the cells expressing Cx50 + AQP0-R33C was significantly reduced (16%; Fig. 7B, # $P < 0.001$)) compared to cells expressing Cx50 + WT-AQP0, indicating mutation-induced reduction in cell-to-cell gap junction coupling.

4. Discussion

Development of total lens cataract in a five-generation family comprising 22 affected individuals from China was investigated by Gu et al. (2007). The study consisting of eighteen members of the family had ten individuals with lens cataract, four unaffected individuals, and four spouses. It was identified that the congenital lens cataract phenotype was due to a mutation in the AQP0 gene localized at 12q13.1–14.1. Sequencing of the AQP0 coding region of the affected members revealed a transition of a pyrimidine to another pyrimidine, C > T, at nucleotide 97 in exon 1 (Gu et al., 2007). The transition resulted in the substitution of cysteine (C) with a neutral polar sulfhydryl side group for arginine (R) with a positively charged polar side group at codon 33 (p.R33C), located in the putative 1st Extracellular Loop (Loop A; Fig. 1B) of AQP0.

AQP0 is the predominant protein in lens fiber cell membranes, constituting ~44.8% of total plasma membrane proteins (Bassnett et al., 2009). In the avascular lens this protein functions as a water channel (Varadaraj et al., 1999, 2005, 2010) and as an adhesion molecule which holds fiber cells tightly to each other. The latter property reduces extracellular space for necessary adjustments to the refractive index of the growing lens (Kumari and Varadaraj et al., 2009; Kumari et al., 2011; Varadaraj et al., 2010). Water permeability of AQP0 in mammals and other vertebrates except fish (Virkki et al., 2001; Clemens et al., 2013) is remarkably low, about 10-fold less compared to more efficient lens epithelial aquaporin, AQP1 (Chandy et al., 1997; Yang and Verkman, 1997). Low water permeability has been speculated to favor dual-functional status of AQP0 as a water pore and cell-to-cell adhesion molecule (Jensen et al., 2008).

Several mutations in the human aquaporin family have been identified as causing inherited diseases (Agre and Kozono, 2003; Verkman, 2008, 2012). Most of these mutations lead to loss of water channel function, and are associated with diseases inherited as autosomal recessive phenotypes except for AQP0. In humans, so far eleven mutations (Table 1a; Fig 1B) have been identified in lens AQP0. All eleven mutations resulted in the dominant phenotype, congenital lens cataract. In mouse, four mutations (Table 1b; Fig 1B) and knockout of AQP0 resulted in autosomal dominant congenital lens cataract. Loss of 50% of AQP0 protein as in the case of heterozygous AQP0 knockout mouse model caused lens cataract suggesting a critical role for AQP0 in lens transparency and homeostasis (Al-Ghoul et al., 2003; Kumari et al., 2011; Shiels et al., 2001; Varadaraj et al., 2010).

Among the eleven mutations identified, only four have been functionally characterized (E134G, T138R (Francis et al., 2000); G213Vfs*45 (Varadaraj et al., 2008); G165D (Senthil Kumar et al., 2013)) thus far. In the present study, we have characterized AQP0-R33C

missense mutation (Gu et al., 2007) that causes autosomal dominant lens cataract in humans. This is the first mutation identified from the Extracellular Loop A of AQP0 that causes lens cataract. Previously characterized mutant AQP0 proteins (Francis et al., 2000; Senthil Kumar et al., 2013; Varadaraj et al., 2008) were unable to traffic and reach the plasma membrane, being trapped mainly in the endoplasmic reticulum (ER) of heterologous expression systems; accumulation of the mutant protein caused ER stress (Senthil Kumar et al., 2013; Varadaraj et al., 2008) due to unfolded protein response, which has been suggested as the reason for pathogenesis of several diseases (Kitamura, 2008; Lin and Lavail, 2010; Reneker et al., 2011; Roussel et al., 2013; Wang et al., 2012). The present study has shown that unlike AQP0 mutants that had been already characterized, AQP0-R33C did not get trapped in the cellular organelle/s and was able to reach the plasma membrane through proper trafficking. Functional characterization of the protein showed that AQP0-R33C retained water channel function as in the case of wild type AQP0, when a comparable amount of the mutant cRNA was injected into the *Xenopus* frog oocytes. All four AQP0 mutants previously studied showed loss of water channel function as a result of impaired membrane trafficking and localization.

We tested for the cell-to-cell adhesion of AQP0-R33C. To our knowledge, this is the first study that has tested cell-to-cell adhesion capability of an AQP0 mutant protein, owing to the undeterred membrane trafficking and water channel function in spite of the mutation. Using a traditional method (Vicker and Edwards, 1972; Takeichi, 1977; Takahashi, et al., 1999; Andl et al., 2003; Hiroaki et al., 2006) and our previously devised method (Kumari and Varadaraj, 2009) to test the cell-to-cell adhesion capability of wild type AQP0, we found that there is ~18%, 27% or 34% decrease in cell-to-cell adhesion capability of this mutant AQP0, presumably due to loss of a positively charged residue in the Extracellular Loop A. The difference in percentage decrease in cell-to-cell adhesion (~18% and ~27% and ~34%) is due to differences in the sensitivity of techniques used; however, the decrease in cell-to-cell adhesion obtained using each technique was statistically significant when compared to cell-to-cell adhesion exhibited by WT-AQP0. Co-expression of WT-AQP0 and AQP0-R33C proteins showed reduction in cell-to-cell adhesion compared to WT-AQP0 that was expressed alone or increase in adhesion compared to AQP0-R33C that was expressed alone (Fig.6A,B), and gave positive FRET signals (Fig. 4a–c), suggesting wild type and mutant channel proteins possibly formed mixed tetramers. While the experiments performed here do not directly measure the cell-to-cell adhesive force involved, they clearly indicate that the force with which the WT-AQP0-expressing cells adhere to each other is compromised in the mutant-protein- expressing cells; considerable number of the latter cells, that had weak adherence, detached during the washing step which represents an applied force. It is noteworthy that the mutation involves loss of a positive charge. Structural and simulation studies have suggested possible involvement of Extracellular Loops of AQP0 in cell-to-cell adhesion of fiber cells (Gonen et al., 2004, 2005; Harries et al., 2004; Jensen et al. 2008; Michea et al., 1994, 1995; Scheuring et al., 2007). Our data show that while arginine in the Extracellular Loop A of AQP0 may not be critical for protein trafficking, localization or water permeability, it appears to be a key player in cell-to-cell adhesion, which is necessary to establish the compact architectural arrangement of fiber cells normally exhibited on lens cross sections.

Previously, we developed a transgenic mouse model in which AQP1 was expressed in lens fiber cells of AQP0 knockout mouse, to test whether transgenic AQP1 can restore lens transparency in cataractous lenses of null mice (Varadaraj et al., 2010); only partial restoration of lens transparency was achieved despite compensation of water permeability by the more efficient water channel AQP1. Electron microscopic studies showed lack of cell-to-cell adhesion in the transgenic lens (Kumari et al., 2011) as observed in the case of AQP0 knockout lens fiber cells (Al-Ghoul et al., 2003). Our *in vitro* and *in vivo* studies showed that

AQP0 is capable of promoting cell-to-cell adhesion in contrast to AQP1 (Kumari and Varadaraj, 2009; Varadaraj et al., 2010; Kumari et al., 2011). Since AQP0-R33C exhibited membrane localization and water permeability comparable to those of WT-AQP0, and reduction in cell-to-cell adhesion, it is reasonable to infer that the decrease in cell-to-cell adhesion may be responsible for causing lens cataract in patients with AQP0-R33C mutation. The fiber cells need to be packed in such a way that intercellular space between two fibers is less than the wavelength of visible light, so that the lens can remain transparent by reducing light scattering.

One of our earlier studies that dealt with spatial and temporal expression of AQP0 and AQP1 during lens development (Varadaraj et al., 2007) indicates that presence of AQP0 is crucial from the beginning. Concomitant with appearance of primary fiber cells as early as Embryonic day (E) 11.25, AQP0 begins to express; this expression continues into secondary fiber cells which differentiate from equatorial epithelial cells. AQP0 expression is constitutive and continues throughout adult life. Even though the epithelial layer is formed first during lens development, AQP1 expression starts only at E17.5, after AQP0 expression at E11.25. Shiels et al (2001) reported that removal of 50% of AQP0 protein as in the case of heterozygous knockout mouse (loss of 50% of the positive charges contributed by AQP0) resulted in severe lens cataract and loss of the architectural fiber cell arrangement in the primary fiber cells (similar to that in the homozygous knockout) at E15.5 compared to age-matched wild type lens carrying 100% AQP0 in the fiber cells. Apparently, presence of AQP0 is necessary throughout lens development and beyond, presumably to establish firm cell-to-cell adhesion for ensuring proper focusing and to achieve and maintain lens transparency while methodically accommodating the new fiber cells that are being constantly added throughout life.

Plasma membranes of adjacent fiber cells form fiber junctions. Enriched presence of AQP0 as square arrays is characteristic of the 11–13 nm junctions seen towards the center of the lens (Zampighi et al., 1989); the intercellular space measures 0.5–0.7 nm, which is much narrower than that in gap junctions (3–5 nm) (Lo and Harding, 1984; Costello et al., 1989; Fitzgerald et al., 1985; Zampighi et al., 1989, 1992). This has been attributed by Michea et al., (1994, 1995) to possible interaction between positively charged amino acids in the extracellular loops of AQP0, and the negatively charged lipid molecules in the adjacent cell membrane. The positively charged amino acid at position 33, in the Extracellular Loop A is highly conserved among vertebrates. In mammals, arginine-33 in the Extracellular Loop A is highly conserved except in platypus, where it is replaced by another positively charged amino acid, histidine (review: Chepelinsky, 2009). Among other vertebrate groups, like in amphibians, this arginine is replaced by a positively charged residue lysine. It must be noted that evolutionarily, the positive charge was conserved. In AQP0-R33C monomer, there is loss of one positive charge due to replacement with cysteine. The development of lens cataract in humans suggests that charged residue at this position is required for function.

Each cell in a vertebrate lens is connected to the adjacent cell via gap junctions (Goodenough, 1992; Mathias et al., 1997). Cataract due to most of the Cx50 mutations is dominant (Beyer et al., 2013; Jiang, 2013), which accentuates the physiological relevance of these channels for lens transparency. The significant roles played by Cx46 and Cx50 in maintaining lens transparency and organ development have been reported through studies on genetically engineered mouse models (Gong et al., 1997; Rong et al., 2002; White et al., 1998). Liu et al. (2011) have shown that gap junction coupling of Cx50 increased when cotransfected with AQP0 compared to cells transfected with only Cx50, due to the cell-to-cell adhesion property of AQP0. In the current investigation, we found that when AQP0-R33C was cotransfected with Cx50, there was significant reduction in cell-to-cell gap junction coupling compared to cells cotransfected with Cx50 and WT-AQP0. While our data

corroborate that AQP0-induced cell-to-cell adhesion facilitates gap junction coupling, they highlight the mutation-induced adverse effect on gap junction coupling due to reduction in cell-to-cell adhesion. Decrease in gap junction coupling could adversely affect the intercellular communication necessary for lens microcirculation to maintain transparency and homeostasis.

The schematic models (Fig. 8) illustrate the possible mechanisms by which decreased cell-to-cell adhesion of the mutant AQP0-R33C might have caused total lens cataract in humans. It is well-documented that in order to be functional, the AQP0 monomers need to be oligomerized into tetramers, even though each monomer can function as an individual channel (Cheng et al., 1997; Murata et al., 2000; Ren et al., 2000; Walz et al., 1997). Five positive charges are present in the extracellular loops of each AQP0 monomer (Fig. 1A). Figure 8, upper panel demonstrates the positive charges in the extracellular domains (20 per tetramer contributed by all 12 extracellular loops) of the WT-AQP0 tetramer being able to interact with the negative charges of lipid membrane, making adjacent fibers come closer and adhere to each other to reduce extracellular space. The adherence of the adjacent plasma membranes in turn permits hemichannels of lens fiber cell gap junction connexons, such as those in Cx46 and Cx50, to come together and form connexin gap junction channels facilitating intercellular communication. Figure 8, lower panel demonstrates that substitution of the positively charged arginine with cysteine (R33C) causes loss of four positive charges (one / monomer) from each tetramer, decreasing the total number of positive charges in the loops to sixteen. The loss of four positive charges per tetramer weakens the drawing and holding forces of AQP0, of the opposing membranes. As a result, the interaction between positive charges of the Extracellular Loop A domains with the negative charges of lipids from opposing plasma membrane becomes compromised, and the extracellular space becomes wider compared to that in the WT-AQP0. Reduced cell-to-cell adhesion may have affected coupling of lens gap junction channels (Cx46 and Cx50) and possible interactions between other proteins/lipids of neighboring fiber cells. Deficiencies in intercellular communication and interactions with other proteins/lipids may have led to defective microcirculation and loss of homeostasis, eventually causing lens cataract. However, we are not ruling out possible unknown function(s) of AQP0 that may have been compromised due to this mutation.

Our inference can be applied to age-related cataract. The continually growing crystalline lens harbors the oldest fiber cells at the center of the lens. With age progression and less or no protein turn-over in the lens mature fiber cells, AQP0 is susceptible to post-translational modifications (PTMs) because of exposure to natural radiations as well as free radicals released during oxidative biological processes. Numerous age-related PTMs have been identified, including deamidation (Ball et al., 2004; Schey et al., 2000), phosphorylation (Ball et al., 2004), N- and C-terminal truncations (Ball et al., 2004; Schey et al., 2000), carbamylation, acetylation, and oleoylation (Gutierrez et al., 2011). For example, deamidation of an asparagine introduces a negative charge on the protein. AQP0 has 4 potential asparagines at positions 115, 119, 197 and 200 which could undergo deamidation during aging. Addition of more negative charges alters the net charge composition of positively charged extracellular domains. This could cause repulsion between deamidation-introduced negative charges of AQP0 and negative charges of fiber cell membrane lipids leading to loss of fiber cell-to-fiber cell adhesion.

In conclusion, among AQP0 mutations characterized thus far, AQP0-R33C is the only mutation that causes autosomal dominant congenital lens cataract in humans, most probably due to loss of cell-to-cell adhesion rather than impaired protein trafficking and loss of water channel function. This mutation further emphasizes the importance of positive charge in Extracellular Loop A at position 33, which is conserved among vertebrate lens AQP0s, for

maintaining lens transparency. Our study suggests that AQP0 tetramers in the fiber cells of opposing membranes help to establish firm and tight cell-to-cell adhesion by electrostatic attraction between positive charges in extracellular loops and negative charges of fiber cell membrane lipids. The physiological role of positive charges in extracellular loops of AQP0 in the lens warrants further investigation by developing mouse models, and will be a direction of our future research.

Acknowledgments

Funding

This work was supported by NIH - NEI grant R01: EY20506.

Abbreviations

WT-AQP0	wild type human Aquaporin 0
AQP1	Aquaporin 1
AQP0-R33C	Aquaporin 0 R33C mutant
FRET	Forster Resonance Energy Transfer
Pw	Water Permeability

References

Aerts T, Xia JZ, Slegers H, de Block J, Clauwaert J. Hydrodynamic characterization of the major intrinsic protein from the bovine lens fiber membranes: extraction in n-octyl-beta-D-glucopyranoside and evidence for a tetrameric structure. J. Biol. Chem. 1990; 265:8675–8680. [PubMed: 2341401]

Agre P, Kozono D. Aquaporin water channels: molecular mechanisms for human diseases. FEBS Lett. 2003; 555:72–78. [PubMed: 14630322]

Al-Ghoul KJ, Kirk T, Kuszak AJ, Zoltoski RK, Shiels A, Kuszak JR. Lens structure in MIP-deficient mice. Anat. Rec. A Discov. Mol. Cell. Evol. Biol. 2003; 273:714–730. [PubMed: 12845708]

Andl CD, Mizushima T, Nakagawa H, Oyama K, Harada H, Chruma K, Herlyn M, Rustgi AK. Epidermal growth factor receptor mediates increased cell proliferation, migration, and aggregation in esophageal keratinocytes *in vitro* and *in vivo* . J. Biol. Chem. 2003; 278:1824–1830. [PubMed: 12435727]

Ball LE, Garland DL, Crouch RK, Schey KL. Post-translational modifications of aquaporin 0 (AQP0) in the normal human lens: spatial and temporal occurrence. Biochemistry. 2004; 43:9856–9865. [PubMed: 15274640]

Bassnett S, Wilmarth PA, David LL. The membrane proteome of the mouse lens fiber cell. Mol. Vis. 2009; 15:2448–2463. [PubMed: 19956408]

Berry V, Francis P, Kaushal S, Moore A, Bhattacharya S. Missense mutations in MIP underlie autosomal dominant 'polymorphic' and lamellar cataracts linked to 12q. Nat. Genet. 2000; 25:15–17. [PubMed: 10802646]

Beyer EC, Ebihara L, Berthoud VM. Connexin mutants and cataracts. Front. Pharmacol. 2013; 4:43. [PubMed: 23596416]

Broekhuyse RM, Kuhlmann ED, Stols AL. Lens membranes II. Isolation and characterization of the main intrinsic polypeptide (MIP) of bovine lens fiber membranes. Exp. Eye Res. 1976; 23:365–371. [PubMed: 976377]

Buck TM, Wagner J, Grund S, Skach WR. A novel tripartite motif involved in aquaporin topogenesis, monomer folding and tetramerization. Nature Struct. Mol. Biol. 2007; 14:762–769. [PubMed: 17632520]

Buzhynskyy N, Hite RK, Walz T, Scheuring S. The supramolecular architecture of junctional microdomains in native lens membranes. EMBO Rep. 2007; 8:51–55. [PubMed: 17124511]

Chandy G, Zampighi GA, Kreman M, Hall JE. Comparison of the water transporting properties of MIP and AQP1. J. Membr. Biol. 1997; 159:29–39. [PubMed: 9309208]

Cheng A, van Hoek AN, Yeager M, Verkman AS, Mitra AK. Three-dimensional organization of a human water channel. Nature. 1997; 387:627–630. [PubMed: 9177354]

Chepelinsky AB. Structural function of MIP/aquaporin 0 in the eye lens; genetic defects lead to congenital inherited cataracts. Handb. Exp. Pharmacol. 2009; 190:265–297. [PubMed: 19096783]

Clemens DM, Németh-Cahalan KL, Trinh L, Zhang T, Schilling TF, Hall JE. In vivo analysis of aquaporin 0 function in zebrafish: permeability regulation is required for lens transparency. Invest. Ophthalmol. Vis. Sci. 2013; 54:5136–5143. [PubMed: 23800763]

Costello MJ, McIntosh TJ, Robertson JD. Membrane specializations in mammalian lens fiber cells: distribution of square arrays. Curr. Eye Res. 1985; 4:1183–1201. [PubMed: 4075818]

El-Fouly MH, Trosko JE, Chang CC. Scrape-loading and dye transfer. A rapid and simple technique to study gap junctional intercellular communication. Exp. Cell Res. 1987; 168:422–430. [PubMed: 2433137]

FitzGerald PG, Bok D, Horwitz J. The distribution of the main intrinsic membrane polypeptide in ocular lens. Curr. Eye Res. 1985; 4:1203–1218. [PubMed: 3907985]

Francis PJ, Berry V, Moore AT, Bhattacharya S. Lens biology: development and human cataractogenesis. Trends Genet. 1999; 15:191–196. [PubMed: 10322486]

Francis P, Chung JJ, Yasui M, Berry V, Moore A, Wyatt MK, Wistow G, Bhattacharya SS, Agre P. Functional impairment of lens aquaporin in two families with dominantly inherited cataracts. Hum. Mol. Genet. 2000; 9:2329–2334. [PubMed: 11001937]

Geyer DD, Spence MA, Johannes M, Flodman P, Clancy KP, Berry R, Sparkes RS, Jonsen MD, Isenberg SJ, Bateman JB. Novel single-base deletional mutation in major intrinsic protein (MIP) in autosomal dominant cataract. Am. J. Ophthalmol. 2006; 141:761–763. [PubMed: 16564824]

Gonen T, Sliz P, Kistler J, Cheng Y, Walz T. Aquaporin-0 membrane junctions reveal the structure of a closed water pore. Nature. 2004; 429:193–197. [PubMed: 15141214]

Gonen T, Cheng YF, Sliz P, Hiroaki Y, Fujiyoshi Y, Harrison SC, Walz T. Lipid-protein interactions in double-layered two-dimensional AQPO crystals. Nature. 2005; 438:633–638. [PubMed: 16319884]

Gong X, Li E, Klier G, Huang Q, Wu Y, Lei H, Kumar NM, Horwitz J, Gilula NB. Disruption of alpha3 connexin gene leads to proteolysis and cataractogenesis in mice. Cell. 1997; 91:833–843. [PubMed: 9413992]

Goodenough DA. The crystalline lens. A system networked by gap junctional intercellular communication. Semin. Cell Biol. 1992; 3:49–58. [PubMed: 1320431]

Grey AC, Walker KL, Petrova RS, Han J, Wilmarth PA, David LL, Donaldson PJ, Schey KL. Verification and spatial localization of aquaporin-5 in the ocular lens. Exp. Eye Res. 2013; 108:94–102. [PubMed: 23313152]

Gu F, Zhai H, Li D, Zhao L, Li C, Huang S, Ma X. A novel mutation in major intrinsic protein of the lens gene (MIP) underlies autosomal dominant cataract in a Chinese family. Mol. Vis. 2007; 13:1651–1656. [PubMed: 17893667]

Gutierrez DB, Garland D, Schey KL. Spatial analysis of human lens aquaporin-0 post-translational modifications by MALDI mass spectrometry tissue profiling. Exp. Eye Res. 2011; 93:912–920. [PubMed: 22036630]

Hamann S, Zeuthen T, La Cour M, Ottersen OP, Agre P, Nielsen S. Aquaporins in complex tissues: distribution of aquaporins 1–5 in human and rat eye. Am. J. Physiol. 1998; 274:C1332–C1345. [PubMed: 9612221]

Harries WE, Akhavan D, Miercke LJ, Khademi S, Stroud RM. The channel architecture of aquaporin 0 at a 2.2-A resolution. Proc. Natl. Acad. Sci. USA. 2004; 101:14045–14050. [PubMed: 15377788]

Hiroaki Y, Tani K, Kamegawa A, Gyobu N, Nishikawa K, Suzuki H, Walz T, Sasaki S, Mitsuoka K, Kimura K, Mizoguchi A, Fujiyoshi AY. Implications of the aquaporin-4 structure on array formation and cell adhesion. J. Mol. Biol. 2006; 355:628–639. [PubMed: 16325200]

Jensen M, Dror R, Xu H, Borhani D, Arkin I, Eastwood M, Shaw D. Dynamic control of slow water transport by aquaporin 0: implications for hydration and junction stability in the eye lens. Proc. Natl. Acad. Sci. U S A. 2008; 105:14430–14435. [PubMed: 18787121]

Jiang JX. Gap junctions or hemichannel-dependent and independent roles of connexins in cataractogenesis and lens development. Curr. Mol. Med. 2010; 10:851–863. [PubMed: 21091421]

Jiang J, Jin C, Wang W, Tang X, Shentu X, Wu R, Wang Y, Xia K, Yao K. Identification of a novel splice-site mutation in MIP in a Chinese congenital cataract family. Mol. Vis. 2009; 15:38–44. [PubMed: 19137077]

Kitamura M. Endoplasmic reticulum stress and unfolded protein response in renal pathophysiology: Janus faces. Am. J. Physiol. Renal Physiol. 2008; 295:F323–F334. [PubMed: 18367660]

Konig N, Zampighi GA, Butler PJ. Characterisation of the major intrinsic protein (MIP) from bovine lens fiber membranes by electron microscopy and hydrodynamics. J. Mol. Biol. 1997; 265:590–602. [PubMed: 9048951]

Kumari SS, Varadaraj K. Intact AQP0 Performs Cell-to-Cell Adhesion. Biochem. Biophys. Res. Commun. 2009; 390:1034–1039. [PubMed: 19857466]

Kumari SS, Eswaramoorthy S, Mathias RT, Varadaraj K. Unique and analogous functions of aquaporin 0 for fiber cell architecture and ocular lens transparency. Biochem. Biophys. Acta. 2011; 1812:1089–1097. [PubMed: 21511033]

Kumari SS, Varadaraj M, Yerramilli VS, Menon AG, Varadaraj K. Spatial expression of aquaporin 5 in mammalian cornea and lens and regulation of its localization by phosphokinase A. Mol. Vis. 2012; 18:957–967. [PubMed: 22550388]

Lin H, Hejtmancik JF, Qi Y. A substitution of arginine to lysine at the COOH-terminus of MIP caused a different binocular phenotype in a congenital cataract family. Mol. Vis. 2007; 13:1822–1827. [PubMed: 17960133]

Lin JH, Lavail MM. Misfolded proteins and retinal dystrophies. Adv. Exp. Med. Biol. 2010; 664:115–121. [PubMed: 20238009]

Liu J, Xu J, Gu S, Nicholson BJ, Jiang JX. Aquaporin 0 enhances gap junction coupling via its cell adhesion function and interaction with connexin 50. J. Cell Sci. 2011; 124:198–206. [PubMed: 21172802]

Lo W-K, Harding CV. Square arrays and their role in ridge formation in human lens fibers. J. Ultrastruct. Res. 1984; 86:228–245. [PubMed: 6544861]

Mathias RT, Rae JL, Baldo GJ. Physiological properties of the normal lens. Physiol. Rev. 1997; 77:21–50. [PubMed: 9016299]

Michea LF, de la Fuente M, Lagos N. Lens major intrinsic protein (MIP) promotes adhesion when reconstituted into large unilamellar liposomes. Biochemistry. 1994; 33:7663–7669. [PubMed: 8011633]

Michea LF, Andrinolo D, Ceppi H, Lagos N. Biochemical evidence for adhesion-promoting role of major intrinsic protein isolated from both normal and cataractous human lenses. Exp. Eye Res. 1995; 61:293–301. [PubMed: 7556493]

Murata K, Mitsuoka K, Hirai T, Walz T, Agre P, Heymann JB, Engel A, Fujiyoshi Y. Structural determinants of water permeation through aquaporin-1. Nature. 2000; 407:599–605. [PubMed: 11034202]

Okamura T, Miyoshi I, Takahashi K, Mototani Y, Ishigaki S, Kon Y, Kasai N. Bilateral congenital cataracts result from a gain-of-function mutation in the gene for aquaporin-0 in mice. Genomics. 2003; 81:361–368. [PubMed: 12676560]

Opsahl H, Rivedal E. Quantitative determination of gap junction intercellular communication by scrape loading and image analysis. Cell Adhes. Commun. 2000; 7:367–375. [PubMed: 10830616]

Ren G, Cheng A, Melnyk P, Mitra AK. Polymorphism in the packing of aquaporin-1 tetramers in 2-D crystals. J. Struct. Biol. 2000; 130:45–53. [PubMed: 10806090]

Reneker LW, Chen H, Overbeek PA. Activation of unfolded protein response in transgenic mouse lenses. Invest. Ophthalmol. Vis. Sci. 2011; 52:2100–2108. [PubMed: 21310900]

Robinson KR, Patterson JW. Localization of steady currents in the lens. Curr. Eye Res. 1983; 2:843–847. [PubMed: 7187641]

Rong P, Wang X, Niesman I, Wu Y, Benedetti LE, Dunia I, Levy E, Gong X. Disruption of Gja8 (alpha8 connexin) in mice leads to microphthalmia associated with retardation of lens growth and lens fiber maturation. Development. 2002; 129:167–174. [PubMed: 11782410]

Roussel BD, Kruppa AJ, Miranda E, Crowther DC, Lomas DA, Marciniak SJ. Endoplasmic reticulum dysfunction in neurological disease. Lancet Neurol. 2013; 12:105–118. [PubMed: 23237905]

Scheuring S, Buzhynskyy N, Jaroslawski S, Gonçalves RP, Hite RK, Walz T. Structural models of the supramolecular organization of AQP0 and connexons in junctional microdomains. J. Struct. Biol. 2007; 160:385–394. [PubMed: 17869130]

Schey KL, Little M, Fowler JG, Crouch RK. Characterization of human lens major intrinsic protein structure. Invest. Ophthalmol. Vis. Sci. 2000; 41:175–182. [PubMed: 10634618]

Senthil Kumar G, Kyle JW, Minogue PJ, Dinesh Kumar K, Vasantha K, Berthoud VM, Beyer EC, Santhiya ST. An MIP/AQP0 mutation with impaired trafficking and function underlies an autosomal dominant congenital lamellar cataract. Exp. Eye Res. 2013; 110:136–141. [PubMed: 23116563]

Shiels A. Focus on Molecules: major intrinsic protein. Exp. Eye Res. 2012; 101:107–108. [PubMed: 21134370]

Shiels A, Bassnett S. Mutations in the founder of the MIP gene family underlie cataract development in the mouse. Nat. Genet. 1996; 12:212–215. [PubMed: 8563764]

Shiels A, Bassnett S, Varadaraj K, Mathias RT, Al-Ghoul K, Kuszak J, Donoviel D, Lilleberg S, Friedrich G, Zambrowicz B. Optical dysfunction of the crystalline lens in aquaporin-0-deficient mice. Physiol. Genomics. 2001; 7:179–186. [PubMed: 11773604]

Sidjanin DJ, Parker-Wilson DM, Neuhauser-Klaus A, Pretsch W, Favor J, Deen PM, Ohtaka-Maruyama C, Lu Y, Bragin A, Skach WR, Chepelinsky AB, Grimes PA, Stambolian DE. A 76-bp deletion in the Mip gene causes autosomal dominant cataract in *Hfi* mice. Genomics. 2001; 74:313–319. [PubMed: 11414759]

Smith BL, Agre P. Erythrocyte Mr 28,000 transmembrane protein exists as a multisubunit oligomer similar to channel proteins. J. Biol. Chem. 1991; 266:6407–6415. [PubMed: 2007592]

Takahashi K, Nakanishi H, Miyahara M, Mandai K, Satoh K, Satoh A, Nishioka H, Aoki J, Nomoto A, Mizoguchi A, Takai Y. Nectin/PRR: an immunoglobulin-like cell adhesion molecule recruited to cadherin-based adherens junctions through interaction with Afadin, a PDZ domain-containing protein. J. Cell Biol. 1999; 145:539–549. [PubMed: 10225955]

Takeichi M. Functional correlation between cell adhesive properties and some cell surface proteins. J. Cell Biol. 1977; 75:464–474. [PubMed: 264120]

Tong J, Canty JT, Briggs MM, McIntosh TJ. The water permeability of lens aquaporin-0 depends on its lipid bilayer environment. Exp. Eye Res. 2013; 113:32–40. [PubMed: 23680159]

Varadaraj K, Kumari S, Mathias RT. Functional expression of aquaporins in embryonic, postnatal, and adult mouse lenses. Dev. Dyn. 2007; 236:1319–1328. [PubMed: 17377981]

Varadaraj K, Kumari S, Mathias RT. Transgenic expression of AQP1 in the fiber cells of AQP0 knockout mouse: effects on lens transparency. Exp. Eye Res. 2010; 91:393–404. [PubMed: 20599966]

Varadaraj K, Kumari S, Shiels A, Mathias RT. Regulation of aquaporin water permeability in the lens. Invest. Ophthalmol. Vis. Sci. 2005; 46:1393–1402. [PubMed: 15790907]

Varadaraj K, Kumari SS, Patil R, Wax MB, Mathias RT. Functional characterization of a human aquaporin 0 mutation that leads to a congenital dominant lens cataract. Exp. Eye Res. 2008; 87:9–21. [PubMed: 18501347]

Varadaraj K, Kushmerick C, Baldo GJ, Bassnett S, Shiels A, Mathias RT. The role of MIP in lens fiber cell membrane transport. J. Membr. Biol. 1999; 170:191–203. [PubMed: 10441663]

Venance L, Piomelli D, Glowinski J, Giaume C. Inhibition by anandamide of gap junctions and intercellular calcium signalling in striatal astrocytes. Nature. 1995; 376:590–593. [PubMed: 7637807]

Verkman AS. Mammalian aquaporins: diverse physiological roles and potential clinical significance. Expert. Rev. Mol. Med. 2008; 10:e13. [PubMed: 18482462]

Verkman AS. Aquaporins in clinical medicine. Annu. Rev. Med. 2012; 63:303–316. [PubMed: 22248325]

Vicker MG, Edwards JG. The effect of neuraminidase on the aggregation of BHK21 ceils and BHK21 cells transformed by polyoma virus. J. Cell Sci. 1972; 10:759–768. [PubMed: 4338905]

Virkki LV, Cooper GJ, Boron WF. Cloning and functional expression of an MIP (AQP0) homolog from killifish (*Fundulus heteroclitus*) lens. Am. J. Physiol. Regul. Integr. Comp. Physiol. 2001; 281:R1994–R2003. [PubMed: 11705786]

Walz T, Hirai T, Murata K, Heymann JB, Mitsuoka K, Fujiyoshi Y, Smith BL, Agre P, Engel A. The three-dimensional structure of aquaporin-1. Nature. 1997; 387:624–627. [PubMed: 9177353]

Wang KJ, Li SS, Yun B, Ma WX, Jiang TG, Zhu SQ. A novel mutation in MIP associated with congenital nuclear cataract in a Chinese family. Mol. Vis. 2011; 17:70–77. [PubMed: 21245956]

Wang S, Kaufman RJ. The impact of the unfolded protein response on human disease. J. Cell Biol. 2012; 197:857–867. [PubMed: 22733998]

Wang W, Jiang J, Zhu Y, Li J, Jin C, Shentu X, Yao K. A novel mutation in the major intrinsic protein (MIP) associated with autosomal dominant congenital cataracts in a Chinese family. Mol. Vis. 2010; 16:534–539. [PubMed: 20361015]

White TW, Goodenough DA, Paul DL. Targeted ablation of connexin50 in mice results in microphthalmia and zonular pulverulent cataracts. J. Cell Biol. 1998; 143:815–825. [PubMed: 9813099]

Xiao X, Li W, Wang P, Li L, Li S, Jia X, Sun W, Guo X, Zhang Q. Cerulean cataract mapped to 12q13 and associated with a novel initiation codon mutation in MIP. Mol. Vis. 2011; 17:2049–2055. [PubMed: 21850180]

Yang B, Verkman AS. Water and glycerol permeabilities of aquaporins 1–5 and MIP determined quantitatively by expression of epitope-tagged constructs in *Xenopus* oocytes. J. Biol. Chem. 1997; 272:16140–16146. [PubMed: 9195910]

Yang G, Zhang G, Wu Q, Zhao J. A novel mutation in the MIP gene is associated with autosomal dominant congenital nuclear cataract in a Chinese family. Mol. Vis. 2011; 17:1320–1323. [PubMed: 21647270]

Yap AS, Brieher WM, Gumbiner BM. Molecular and functional analysis of cadherin-based adherens junctions. Annu. Rev. Cell Dev. Biol. 1997; 13:119–146. [PubMed: 9442870]

Zampighi GA, Simon SA, Hall JE. The specialized junctions of the lens. Int. Rev. Cytol. 1992; 136:185–225. [PubMed: 1506144]

Zampighi GA, Hall JE, Ehring GR, Simon SA. The structural organization and protein-composition of lens fiber junctions. J. Cell Biol. 1989; 108:2255–2275. [PubMed: 2738093]

Highlights

- First report to show R33C mutant AQP0 caused impairment of cell-to-cell adhesion.
- AQP0-R33C mutation did not alter protein trafficking and membrane localization.
- AQP0-R33C mutation did not affect water channel function.
- AQP0-R33C mutation affected Cx50 gap junction coupling.
- Reduced cell-to-cell adhesion could underlie the cataract due to AQP0-R33C mutation.

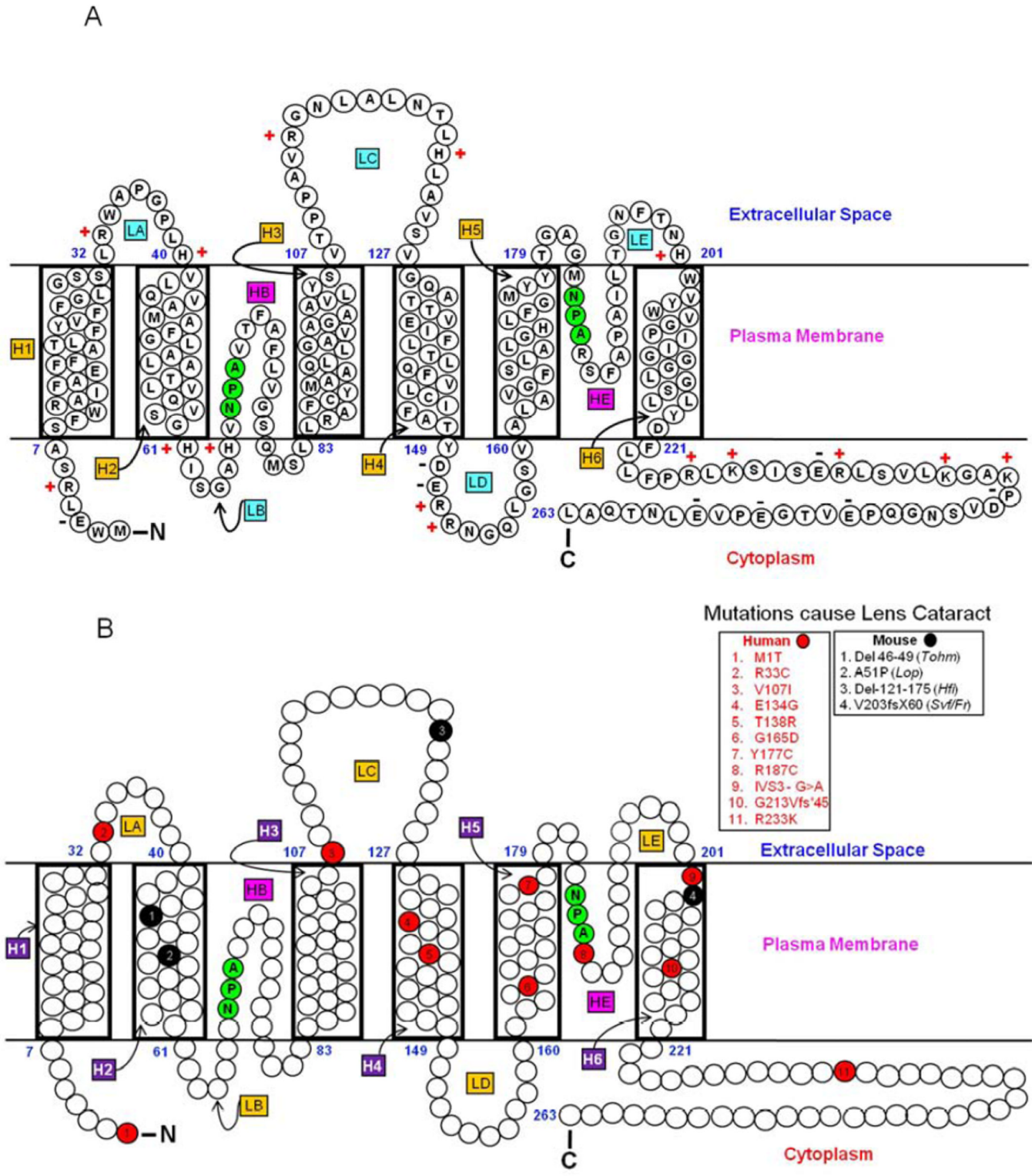

Fig. 1.

(A). Schematic representation of human AQP0. Monomeric structure shows folds, helix assignment, and location in the membrane. Membrane-spanning helices are denoted as H1–H6 and loops as LA–LE. The two pore lining helices are shown as HB and HE. Highly

conserved NPA motifs in loops B and E (shaded green) that line the water pore of aquaporin are shown. NH_2, amino terminus; COOH, carboxy terminus. '+' and '−' represent amino acid charges in extracellular and cytoplasmic domains. **(B)**. AQP0 mutations in humans and mice. Schematic illustration of the locations of eleven mutations in humans (red) and four mutations in mice (black) that cause inherited lens cataracts. AQP0 secondary structure domain designations are as given in (Fig 1A).

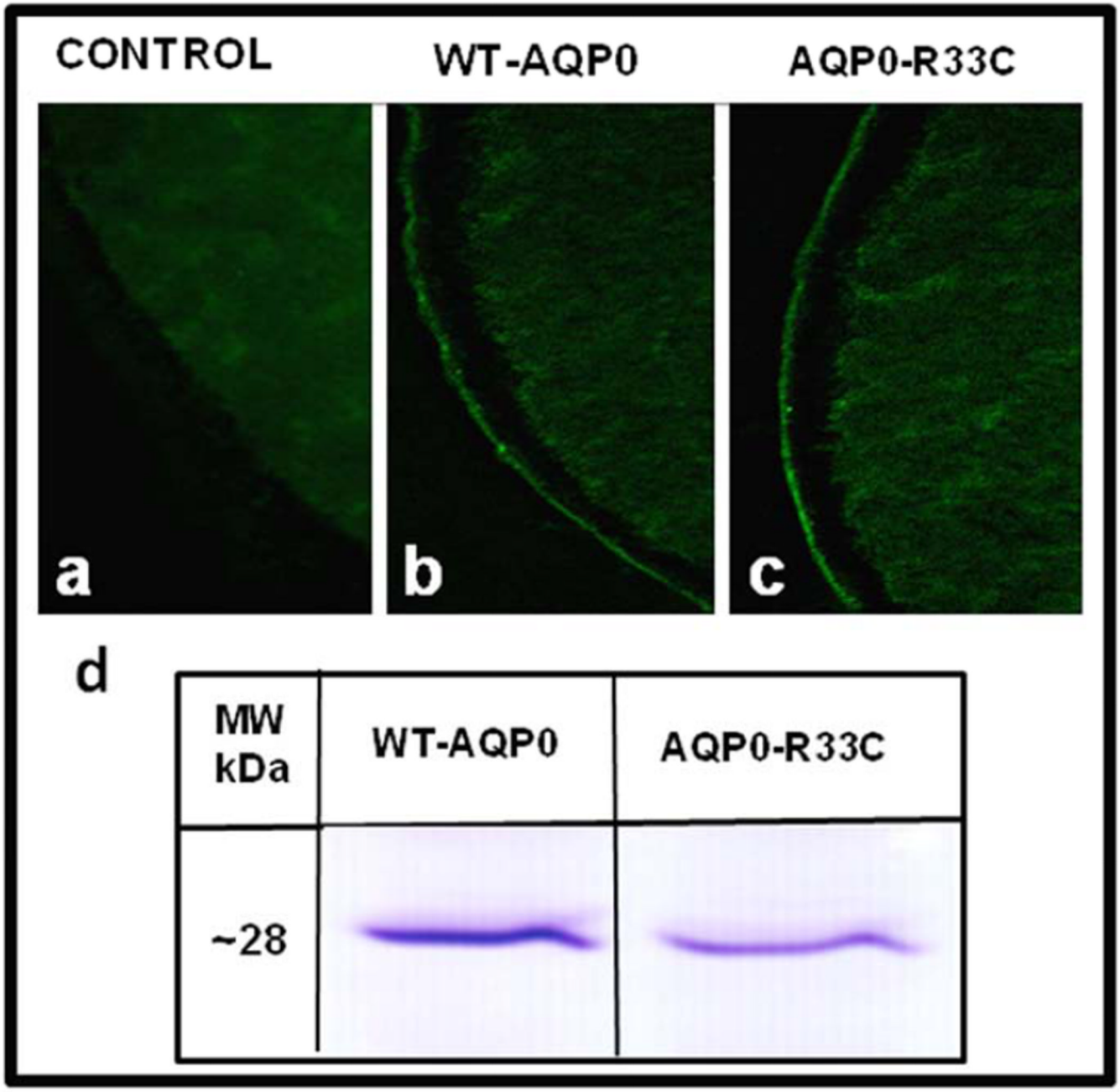

Fig. 2.

Expression of WT-AQP0 and AQP0-R33C in the *Xenopus laevis* oocytes. **(a–c)** Immunostaining of cryosections of oocytes injected with distilled water or AQP0 cRNAs. Expression of WT-AQP0 or mutant AQP0-R33C was visualized by immunostaining using anti-AQP0 antibody: **(a)** Water injected oocytes, **(b)** WT-AQP0 cRNA injected and **(c)** mutant AQP0-R33C cRNA injected oocytes. **(d)** Western blot analysis of oocytes injected with cRNA of WT-AQP0 (lanes 1) or mutant AQP0-R33C (lane 2).

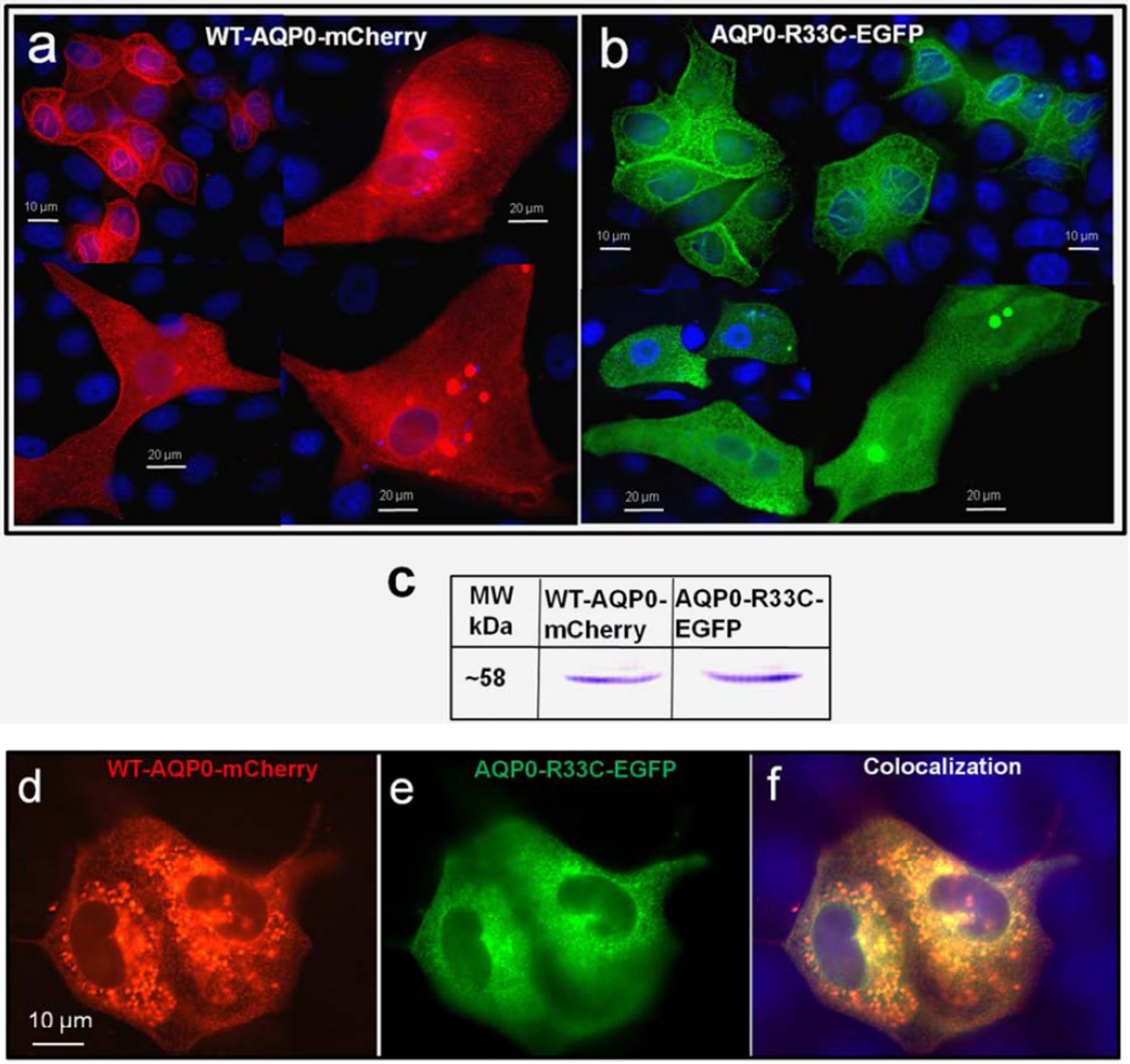

Fig. 3.

Localization and colocalization of WT-AQP0-mCherry and AQP0-R33C-EGFP. (**a, b**) Epifluorescent images of MDCK cells transfected with the WT-AQP0-mCherry and AQP0-R33C-EGFP, respectively. **c**. Western blot analysis of MDCK cells expressing WT-AQP0-mCherry (lane 1) and AQP0-R33C-EGFP (lane 2). **(d–f)** Cells cotransfected with WT-AQP0-mCherry and AQP0-R33C-EGFP constructs; **(d)** cotransfected cell viewed under mCherry fluorescent filter; **(e)** the same cells under an EGFP fluorescent filter; **(f)** overlaid image of **(d)** and **(e)**.

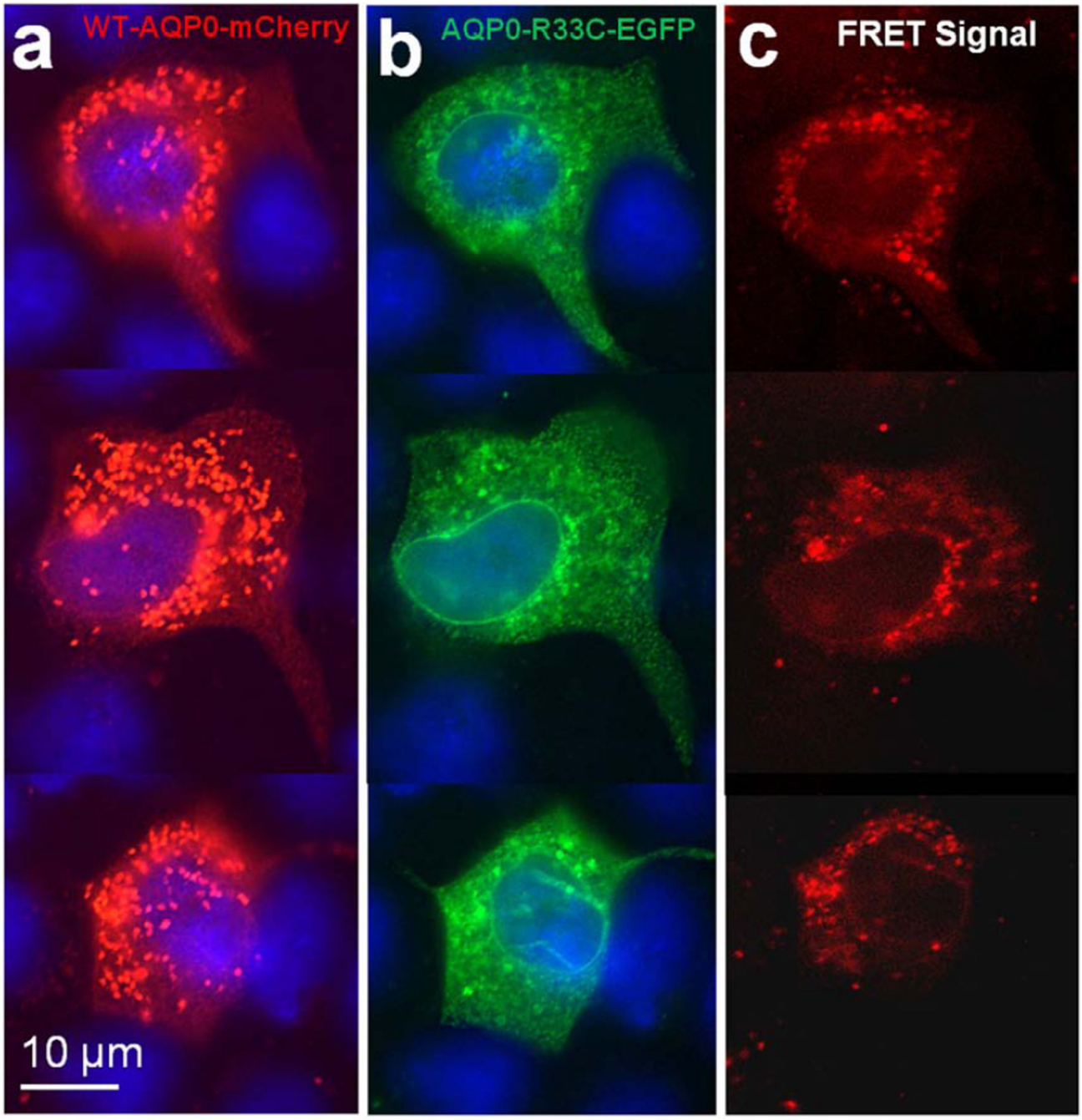

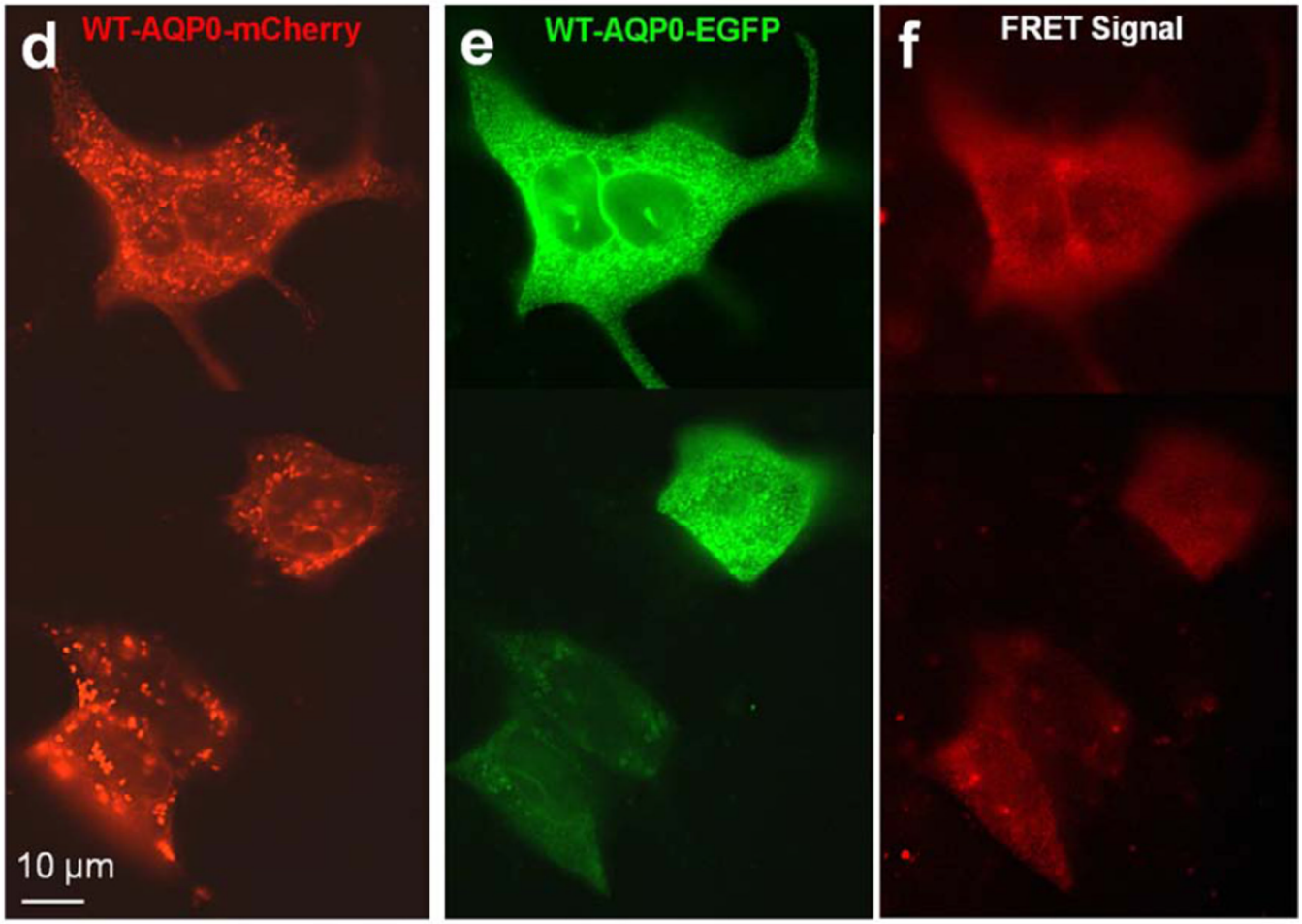

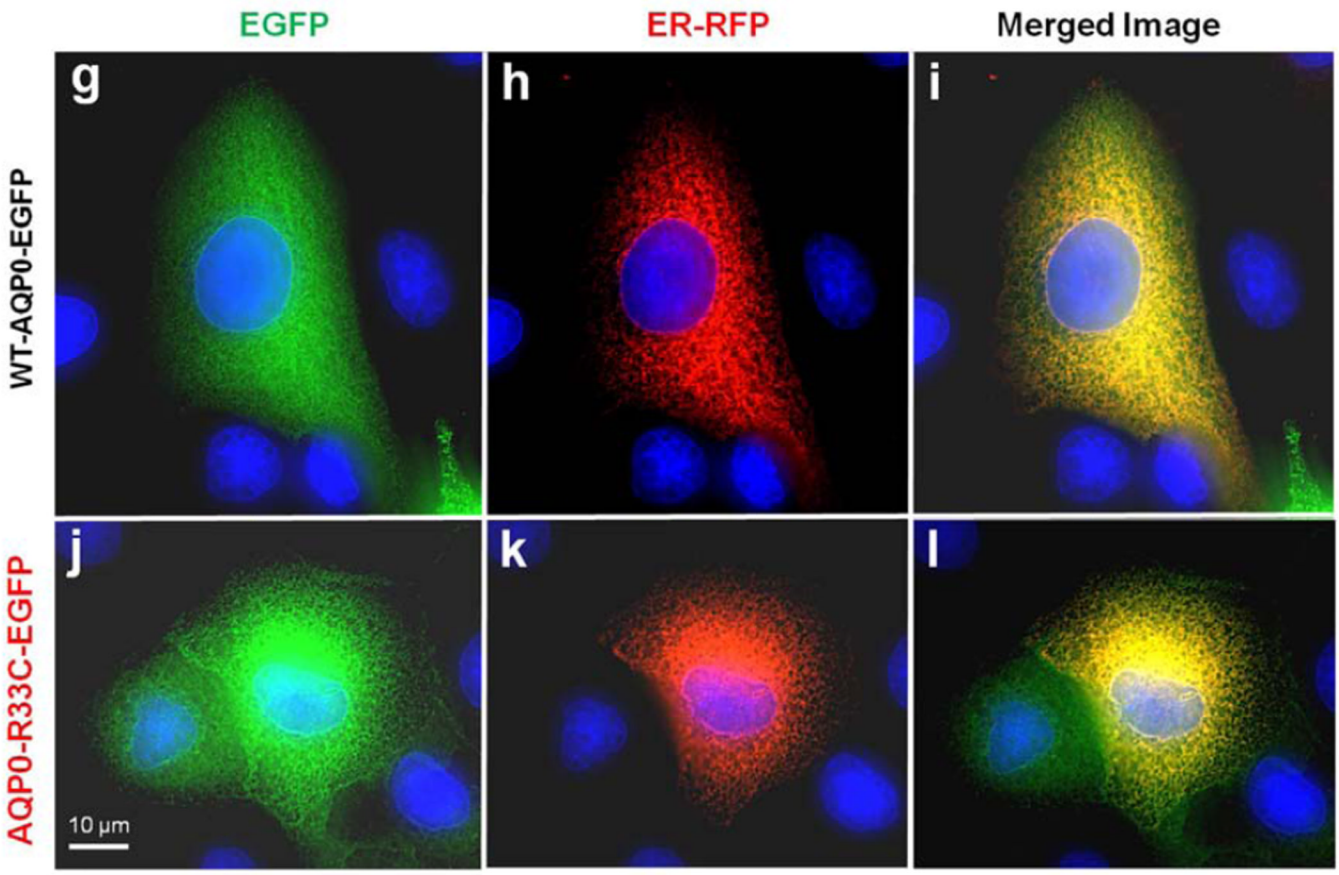

Fig. 4.

Protein colocalization. **(a–f)** Forster Resonance Energy Transfer in MDCK cells cotransfected with WT-AQP0-mCherry and mutant AQP0-R33C-EGFP or WT-AQP0-EGFP and WT-AQP0-mCherry. Cells were cotransfected with: WT-AQP0-mCherry and AQP0-R33C-EGFP **(a–c)**, WT-AQP0-mCherry and WT-AQP0-EGFP **(d–f); (a, d)** cells excited at 587 nm and emission recorded at 610 nm; **(b, e)** cells excited at 488 nm and emission recorded at 507 nm; **(c, f)** cells excited at 470 nm and emission recorded at 640 nm fluorescence due to FRET; **(c, f)** fluorescence indicating colocalization of mutant AQP0-R33C-EGFP and WT-AQP0-mCherry or WT-AQP0-EGFP and WT-AQP0-mCherry proteins in the same oligomer or within 100Å. **(g–i)** Localization of WT-AQP0-EGFP, AQP0-R33C-EGFP in the ER. MDCK cells were coexpressed with WT-AQP0-EGFP or WT-AQP0-mCherry and organelle light ER-RFP. **(g, j)** Images taken under EGFP filter; **(h, k)** images taken under Texas Red filter; **(i, l)** merged images of **(g, h)** and **(j, k)**, respectively showing yellow color due to colocalization of the respective protein (green) in the ER along with the organelle light (red). The green fluorescence at the periphery of the images **(i)** and **(l)** indicates plasma membrane localization of WT-AQP0-EGFP and AQP0-R33C-EGFP, respectively.

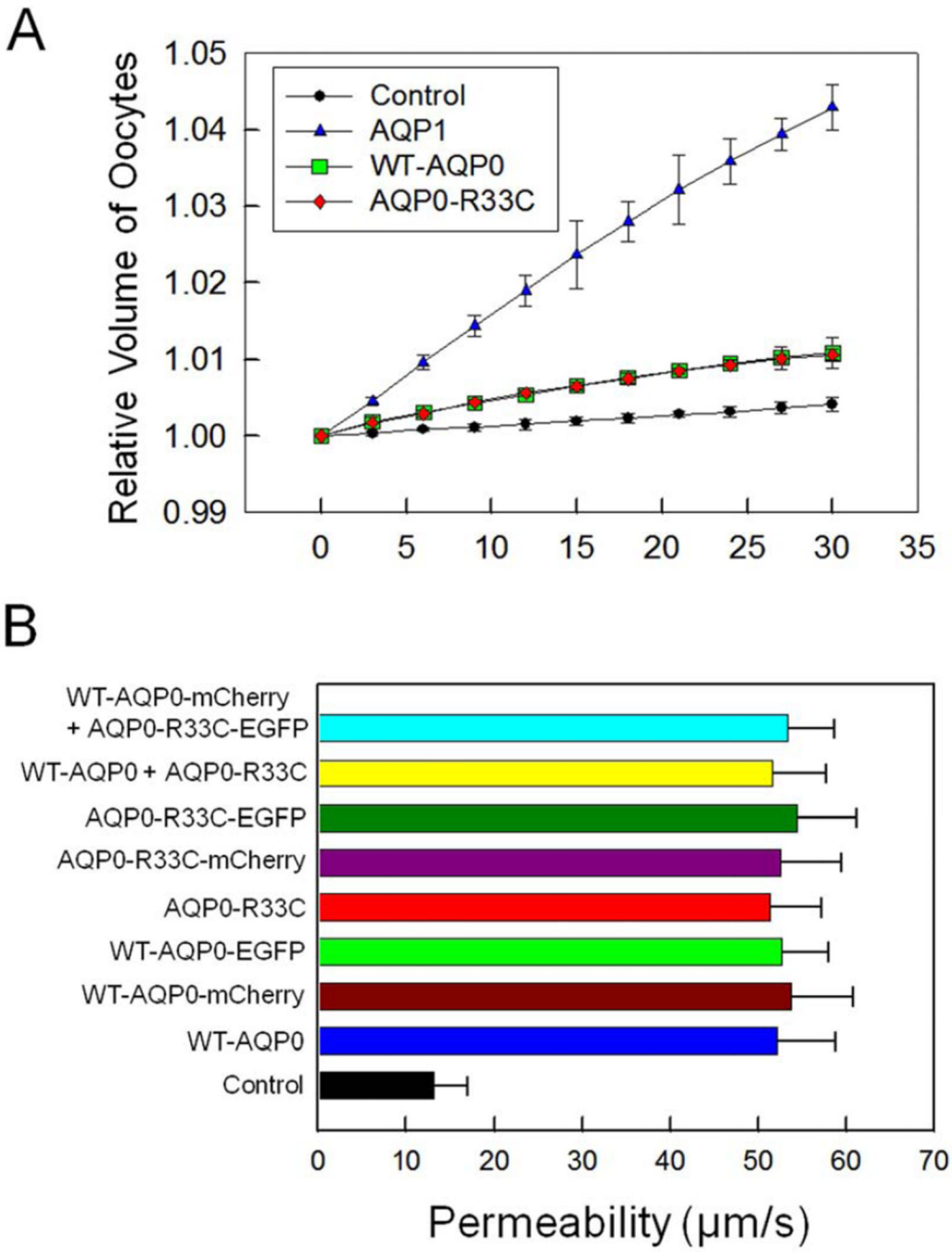

Fig. 5.

Water permeability of WT-AQP0 and AQP0-R33C. **(A)** Membrane water permeability of *Xenopus laevis* oocytes injected with distilled water, 5 ng/oocyte cRNA of WT-AQP1, 25 ng/oocyte cRNA of WT-AQP0 or 25 ng/oocyte cRNA of AQP0-R33C. An oocyte was placed in a hypotonic solution and initial rate of swelling was estimated. A simple curve fit to the data was obtained to calculate the oocyte membrane water permeability as described in the "Materials and Methods' section. Relative volume due to water uptake of oocytes injected with distilled water (control), human AQP1-cRNA, human WT-AQP0-cRNA or human mutant AQP0-R33C-cRNA is plotted. **(B)** Oocyte membrane water permeability of

nine swelling assays (each assay with 15 oocytes; (mean ± SD)). Compared to control all assays showed significant increase in water permeability, $P < 0.0001$. There was no significant difference in water permeability between fluorescent protein tagged and untagged WT-AQP0, AQP0-R33C or WT-AQP0 + AQP0-R33C, $P > 0.05$.

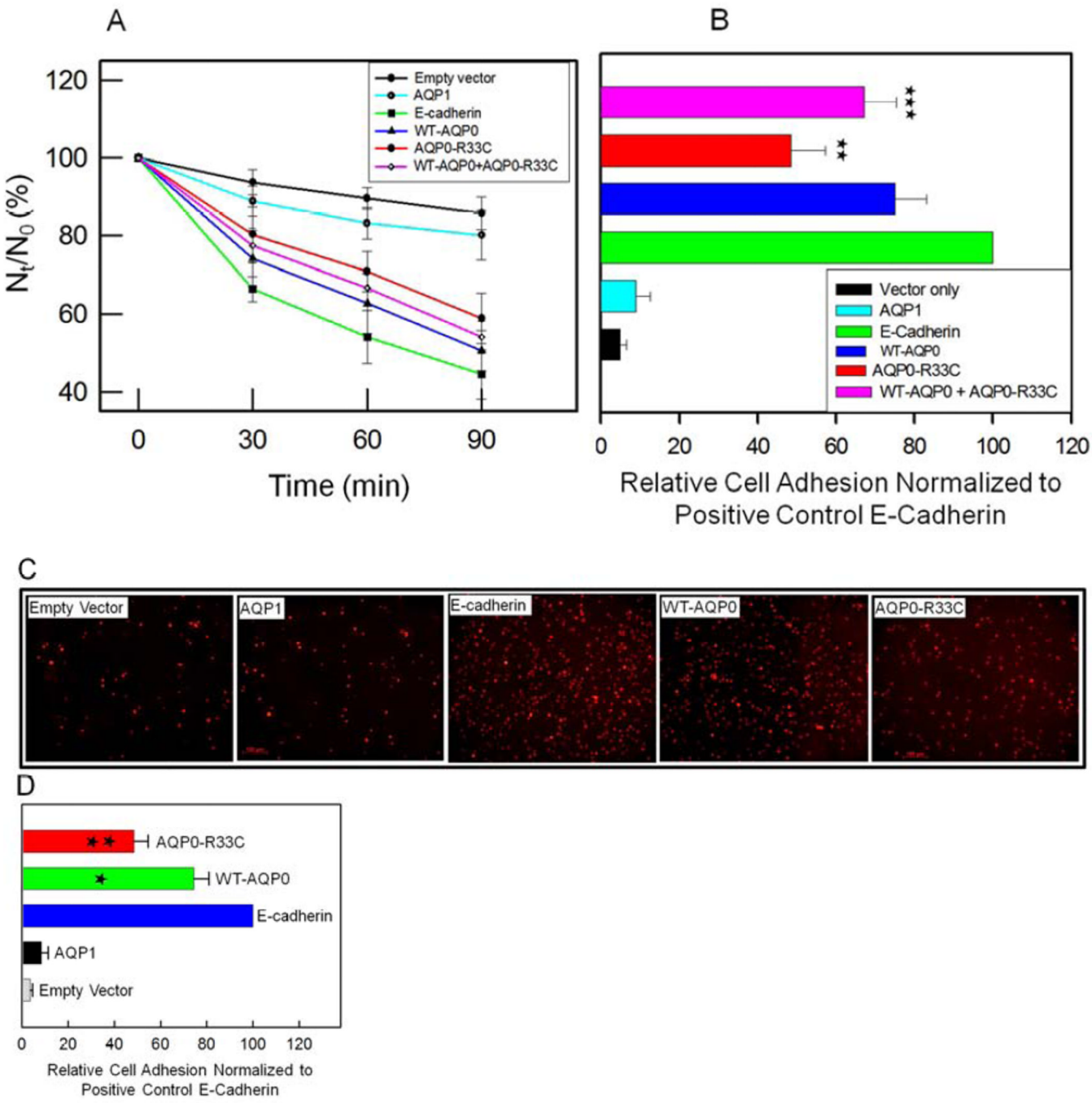

Fig. 6.

Cell aggregation assay using rotary gyratory shaker. **(A)**. Cell aggregation exhibited by adhesion-deficient L-cells expressing empty vector, AQP1, E-cadherin, WT-AQP0, AQP0-R33C or WT-AQP0 + AQP0-R33C in relation to incubation time. (Nt -total number of particles at time 't' of incubation; N_0 - initial number of particles). **(B)**. Cell-to-cell adhesion assay using a microplate reader. Over a monolayer of L-cells expressing empty vector (negative, control), AQP1 (negative, control), E-cadherin (positive control), WT-AQP0, AQP0-R33C or WT-AQP0 + AQP0-R33C corresponding cells loaded with CellTracker Red were plated. A microplate reader was used to obtain data as described in the 'Materials and

Methods' section. Stars (**, ***) indicate statistically significant reduction in cell-to-cell adhesion in AQP0-R33C or WT-AQP0 + AQP0-R33C compared to the WT-AQP0. **(C)**. Cell-to-cell adhesion assay using a fluorescence microscope. Over a monolayer of L-cells expressing empty vector, AQP1, E-cadherin, WT-AQP0 or AQP0-R33C corresponding cells loaded with CellTracker Red were plated. At the end of the procedure described in the 'Materials and Methods' section, cells were imaged under an epifluorescent microscope (Zeiss). Cells/aggregates were counted and values were plotted. **(D)**. Histogram showing the extent of cell-to-cell adhesion exhibited after 45 min. of incubation by samples tested using the fluorescence assay. *Compared to E-Cadherin, WT-AQP0 exhibited significantly low ($P < 0.001$) cell-to-cell adhesion. **Compared to WT-AQP0, mutant AQP0-R33C exhibited significantly low cell-to-cell adhesion.

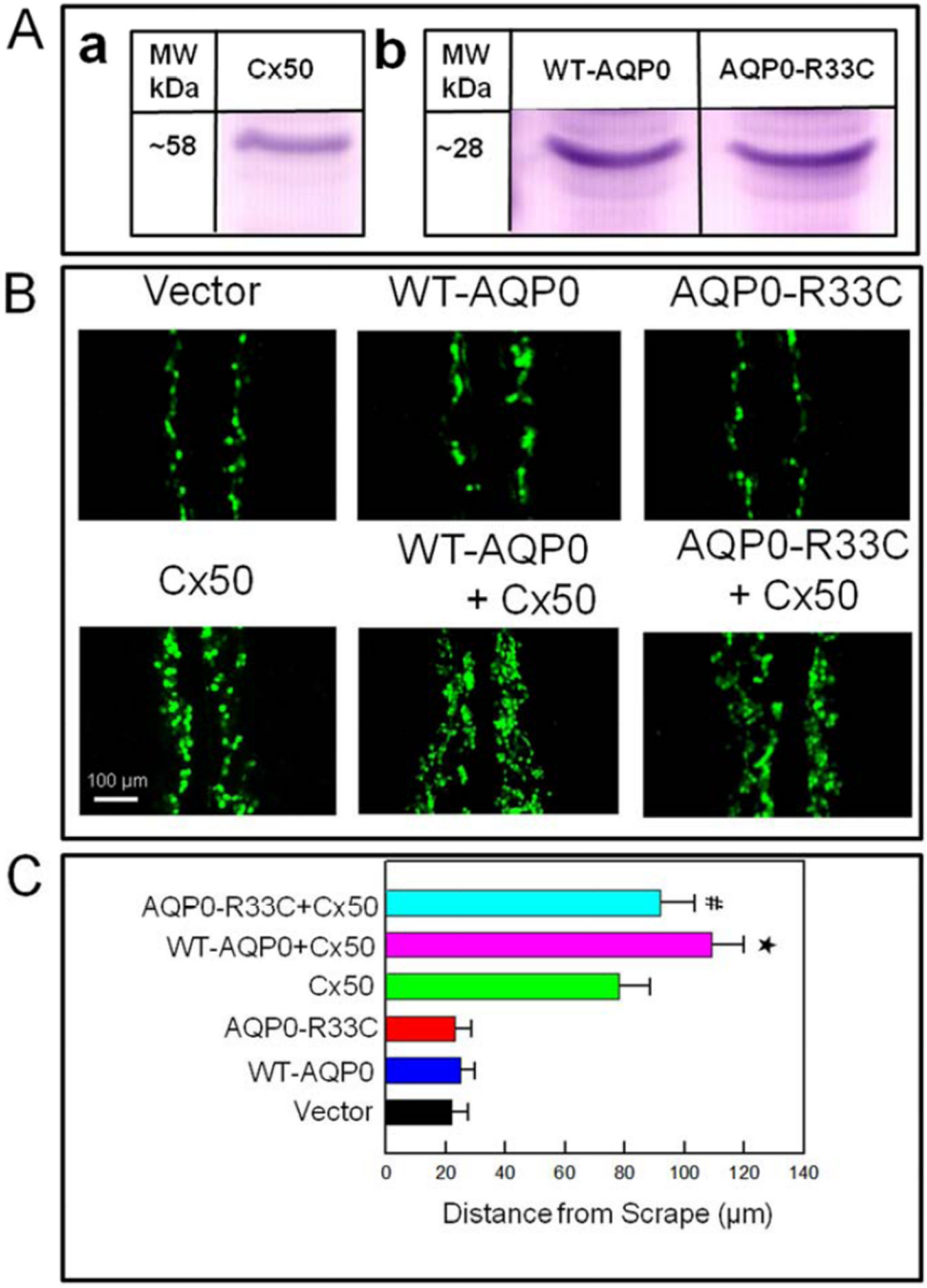

Fig. 7.

Scrape-loading dye transfer assay showing AQP0-facilitated gap junction coupling. (**A**). Western blotting of **(a)** Cx50, **(b)** WT-AQP0 and AQP0-R33C proteins to show expression of the respective proteins on L-cells. **(B)**. Lucifer yellow (LY) dye transfer in L-cells stably expressing vector, WT-AQP0, AQP0-R33C, Cx50, WT-AQP0 + Cx50 or AQP0-R33C + Cx50. The extent of dye transfer was quantified by measuring distance from the scrape line to the dye front of LY. **(C)**. Bar graph representing the data collected, presented as mean ± SD. (*n=5*). ***** Increase in gap junction coupling in WT-AQP0 + Cx50 transfected cells was statistically significant ($P < 0.001$) compared to Cx50 transfected cells; **#** Reduction in gap

junction coupling in AQP0-R33C + Cx50 transfected cells was statistically significant ($P < 0.001$) compared to WT-AQP0 + Cx50 transfected cells.

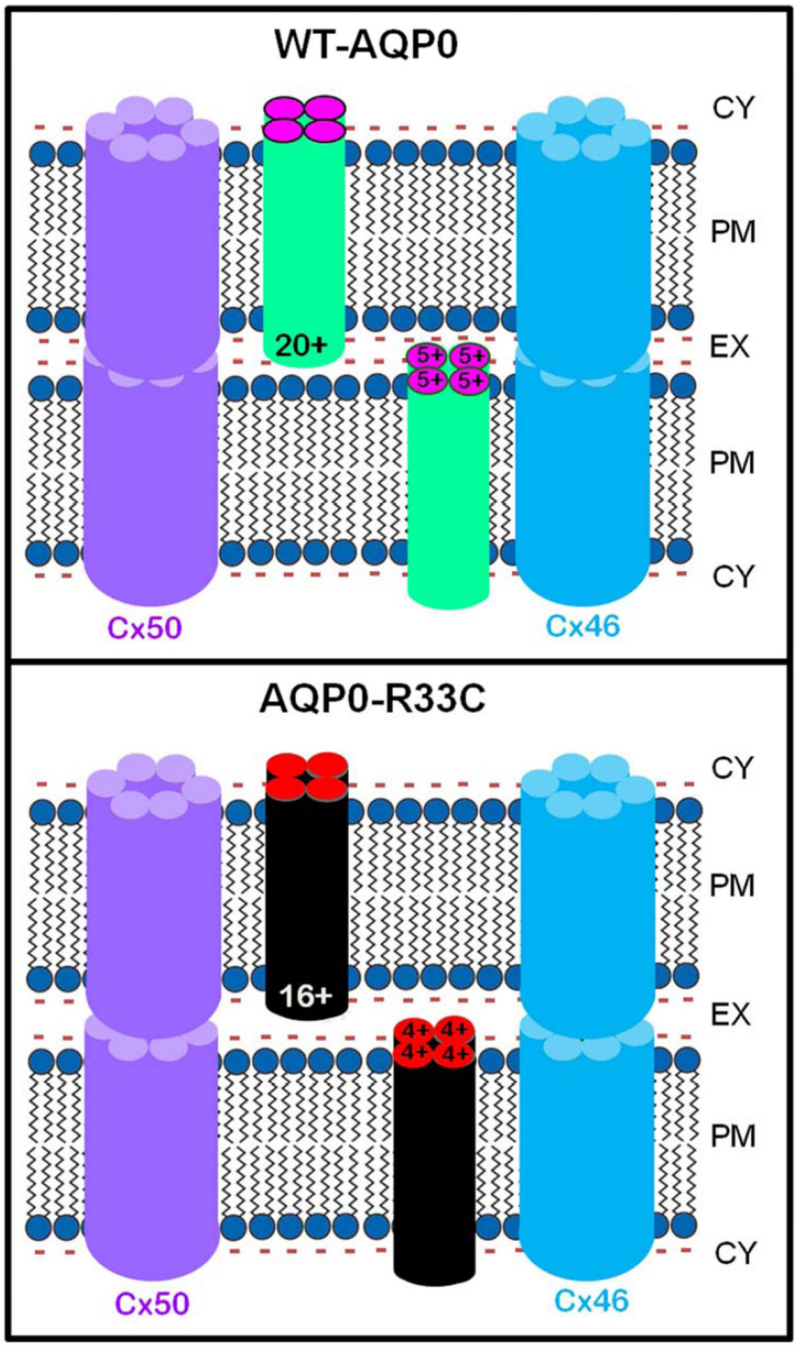

Fig. 8.

Schematic models illustrating the possible cause for autosomal dominant congenital lens cataract due to R33C missense mutation. **WT-AQP0:** It has been postulated that positive charges in the extracellular loops of AQP0 play a significant role in cell-to-cell adhesion. WT-AQP0 monomers form tetramers. Each tetramer carries a total of 20 positive charges (5 / monomer) in Extracellular Loops, A, C and E. These positive charges electrostatically attract negatively charged lipids of the opposing fiber cell plasma membrane to come closer, thus reducing the extracellular space between the fibers and enabling firm and tight cell-to-cell adhesion. The proximity of fiber cells facilitates gap junction hemichannels to couple

and form channels for intercellular communication, which aids in microcirculation and homeostasis of the avascular lens. **R33C-AQP0**: Mutation at codon 33 in the Extracellular Loop A of AQP0 resulted in replacement of positively charged amino acid arginine (R) to a neutral amino acid cysteine (C). Mutant AQP0-R33C tetramer has only 16 positive charges in extracellular loops due to loss of an arginine to cysteine in each monomer. This reduction might have decreased the pulling and holding forces between opposing fiber cells due to the fewer number of positive charges interacting with negative charges of the plasma membrane lipids, leading to wider intercellular space between adjacent fibers compared to that in the WT-AQP0. Reduced cell-to-cell adhesion of AQP0-R33C might have eventually caused loss of gap junction coupling, compromising intercellular communication, microcirculation and homeostasis of the lens.

Table 1

a. Mutations in human AQP0 and characteristics of the resulting lens cataract					
Families with Congenital Lens Cataract	**Mutation in AQP0 gene**	**Specificity of mutation in AQP0 protein**	**Location of the mutation in AQP0 protein**	**Phenotype**	**Reference**
Family A from southern England	Point mutation C to G transversion (exon 2)	Point mutation T138 to R (AQP0 - 263 amino acids (aa))	Transmembrane H4	Polymorphic cataract. Congenital, isolated, progressive, bilateral, punctate lens opacities limited to mid and peripheral lamellae or asymmetric anterior and posterior polar opacification or cortical cataract	Berry et al., 2000
Family B from southeastern England	Point mutation A to G transition (exon 2)	Point mutation E134 to G (AQP0 - 263 aa)	Transmembrane H4	Isolated, non-progressive, congenital lamellar and sutural opacification	Berry et al., 2000
Family ADC2, European descent	One base pair deletion (exon 4)	Frameshift (G213Vfs*45) at codon 213; #213 to 257 aa in frameshift at C-terminus (Shortened AQP0 =257 aa)	Transmembrane H6 and cytoplasmic C-terminus	Congenital bilateral cataract; Embryonic nuclear opacities	Geyer et al., 2006
Chinese Family 1	Point mutation C to T transition (exon 1)	Point mutation R33 to C (AQP0 263 aa)	Extracellular Loop A	Congenital total cataract; bilateral, complete opacification of the fetal nucleus and the cortex	Gu et al., 2007
Chinese Family 2	Point mutation G to A transition (exon 4)	Point mutation R233 to K (AQP0 263 aa)	cytoplasmic C-terminal	Dominant binocular polymorphic cataract	Lin et al., 2007
Chinese Family 3	splice-site mutation (c.607-1 G to A transition)	Premature stop codon, (AQP0 205 aa)	Loss of Transmembrane H6 and cytoplasmic C-terminal	congenital total cataract, snaillike” phenotype	Jiang et al., 2009
Chinese Family 4	Point mutation c.319- G to A transition	Point mutation V107 to I (AQP0 - 263 aa)	Mutation in Extracellular Loop C	Y-suture and nuclear pulverulent opacification; complete opacification in the fetal nuclear region	Wang et al., 2010

a. Mutations in human AQP0 and characteristics of the resulting lens cataract

Families with Congenital Lens Cataract	Mutation in AQP0 gene	Specificity of mutation in AQP0 protein	Location of the mutation in AQP0 protein	Phenotype	Reference
Chinese Family 5	Point mutation C.559 C to T transition	Point mutation R187 to C (AQP0 - 263 aa).	Helix E	Bilateral congenital nuclear cataract	Wang et al., 2011
Chinese Family 6	Point mutation (c. 530 A to G transition)	Point mutation Y177 to C (AQP0 - 263 aa)	Transmembrane H5	Dominant congenital nuclear cataract	Yang et al., 2011
Chinese Family 7	Point mutation c.2 T to C transition	Point mutation at start codon	Mutation affects the initiation codon, ATG, which may result in no protein production or activation of a new translation initiation site	Cerulean cataract with different morphology (lamellar, punctuate, and/or Y-sutural) in different patients	Xiao et al., 2011
South Indian family 1	Point mutation c.494 G to A transition	Point mutation G165 to D (AQP0 - 263 aa)	Transmembrane H5	Congenital lamellar cataract	Senthil Kumar et al., 2013

b. Mutations in mouse AQP0 and characteristics of the resulting lens cataract

Mouse with Congenital Lens Cataract	AQP0 gene Mutation	Specificity of mutation in AQP0 protein	Location of the mutation in AQP0 protein domain*	Phenotype	Reference
Cat^{Fr} *(Fraser)*	Insertion transposon in intron 3/ exon 4 junction	Replacement amino acid (aa) #203 to 263 at C-terminus by transposon sequence (E Tn) (AQP0 - 261 aa)	Transmembrane H6 and cytoplasmic C-terminus	Progressive Lens fiber degeneration and cataractogenesis	Shiels and Bassnett, 1996
Lop (Lens opacity)	Point mutation G to C transversion (exon 1)	Point mutation aa #51 A to P (AQP0 - 263 aa)	Transmembrane H2	Progressive lens fiber cell degeneration and cataractogenesis	Shiels and Bassnett, 1996
Hfi (Hydropic lens)	Deletion of 76 base pair at junction exon 2/ intron 2	Deletion 55 aa #128 to #175 (AQP0 - 208 aa)	Transmembrane H4 and H5, extracellular loop C and intracellular loop D	Heterozygotes with hydropic lens fibers and homozygotes with total lens cataract	Sidjanin et al., 2001

b. Mutations in mouse AQP0 and characteristics of the resulting lens cataract					
Mouse with Congenital Lens Cataract	**AQP0 gene Mutation**	**Specificity of mutation in AQP0 protein**	**Location of the mutation in AQP0 protein domain***	**Phenotype**	**Reference**
Cat^{Tohm} *(Tohoku)*	Deletion of 12 base pair (exon 1)	Deletion aa #46 to 49 (AQP0 259 aa)	Transmembrane H2	Severe lens fiber degeneration and cataractogenesis. Dominant cataract	Okamura et al., 2003

*AQP0 protein domains correspond to those indicated Fig. 1A, B